



Contents lists available at ScienceDirect

Journal of Fluids and Structures

journal homepage: www.elsevier.com/locate/jfs



Numerical investigation of the behaviour and performance of ships advancing through restricted shallow waters

Momchil Terziev^a, Tahsin Tezdogan^{a,*}, Elif Oguz^a, Tim Gourlay^b, Yigit Kemal Demirel^a, Atilla Incecik^a

^a Department of Naval Architecture, Ocean and Marine Engineering, Henry Dyer Building, University of Strathclyde, 100 Montrose Street, Glasgow, G4 0LZ, UK

^b Perth Hydro Pty Ltd, Level 29, 221 St Georges Terrace, Perth, Western Australia, Australia



HIGHLIGHTS

- CFD simulations were run for the DTC in shallow water at various speeds.
- Unrestricted, restricted and dredged channels incorporated.
- Sinkage, trim and resistance measured in Star-CCM+.
- Results were compared to those of SlenderFlow.
- Wave patterns were shown to vary significantly for different channel topographies.

ARTICLE INFO

Article history:

Received 14 June 2017

Received in revised form 25 August 2017

Accepted 3 October 2017

Keywords:

Ship squat

Slender body theory

CFD

Ship resistance

Trim and sinkage

ABSTRACT

Upon entering shallow waters, ships experience a number of changes due to the hydrodynamic interaction between the hull and the seabed. Some of these changes are expressed in a pronounced increase in sinkage, trim and resistance. In this paper, a numerical study is performed on the Duisburg Test Case (DTC) container ship using Computational Fluid Dynamics (CFD), the Slender-Body theory and various empirical methods. A parametric comparison of the behaviour and performance estimation techniques in shallow waters for varying channel cross-sections and ship speeds is performed. The main objective of this research is to quantify the effect a step in the channel topography on ship sinkage, trim and resistance. Significant differences are shown in the computed parameters for the DTC advancing through dredged channels and conventional shallow water topographies. The different techniques employed show good agreement, especially in the low speed range.

© 2017 The Authors. Published by Elsevier Ltd. This is an open access article under the CC BY license (<http://creativecommons.org/licenses/by/4.0/>).

Abbreviations

$b(x)$	Ship beam as a function of position (m)
B	Ship beam amidships (m)
C	Celerity (m/s)
C_B	Block coefficient (-)

* Corresponding author.

E-mail address: tahsin.tezdogan@strath.ac.uk (T. Tezdogan).

C_F	Frictional resistance coefficient (-)
C_m	Moment coefficient (-)
C_M	Midship section coefficient (-)
C_S	Sinkage coefficient (-)
C_T	Total resistance coefficient (-)
C_{WP}	Waterplane coefficient (-)
C_ϑ	Trim coefficient (-)
<i>CFD</i>	Computational Fluid Dynamics
<i>CFL</i>	Convective Courant–Friedrichs–Lowy Number (-)
<i>CoB</i>	Centre of buoyancy (m)
<i>CoG</i>	Centre of gravity (m)
<i>DFBI</i>	Dynamic fluid-body interaction
<i>DTC</i>	Duisburg test case
<i>DWT</i>	Dead weight tonnage
e	Relative error
F_d	Depth Froude number (-)
g	Acceleration due to gravity (9.81 m/s ²)
<i>GCI</i>	Grid convergence index
GM_T	Metacentric height (m)
h	Water depth (m)
<i>ITTC</i>	International Towing Tank Conference
k	Fourier transform variable
<i>KCS</i>	KRISO containership
L	Ship length (m)
p	Refinement ratio
<i>RANS</i>	Reynolds averaged Navier–Stokes
R	Convergence ratio
R_F	Frictional resistance (N)
R_P	Pressure resistance (N)
R_T	Total Resistance (N)
s	Sinkage (m)
S	Blockage factor
$S(x)$	Ship cross sectional area as a function of position (m ²)
S_w	Wetted area (m ²)
t	Trim (rad)
T	Ship draught (m)
<i>TEU</i>	Twenty-foot equivalent unit
V	Velocity (m/s)
<i>VCG</i>	Vertical centre of gravity (m)
<i>VOF</i>	Volume of fluid
w	Channel width (m)
W_{eff}	Effective width of channel (m)
α	Shape constant
β	Shape constant
Δt	Time step (s)
Δx	Length of control volume (m)
ϑ	Trim angle (°)
ρ	Water density (988.1 kg/m ³)
φ	Velocity potential
Φ	General transport variable
∇	Volumetric displacement (m ³)

1. Introduction

Ship behaviour and performance are highly influenced by the hydrodynamic interaction between the hull and the proximity of the seabed. Namely, the flow velocity between the hull's bottom and the seabed increases, which produces a drop in pressure. This can be thought of in terms of the Bernoulli principle, where an increase in kinetic energy causes a decrease in pressure in order to satisfy the energy conservation condition (Debaillon, 2010). The abovementioned pressure

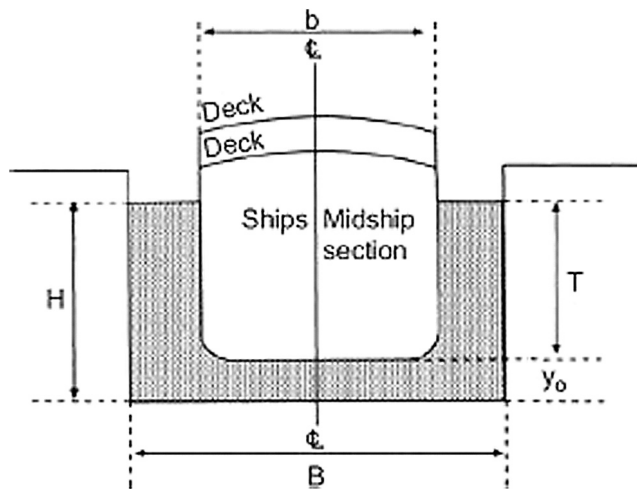


Fig. 1. Blockage factor, taken from Barrass (2012).

reduction creates a vertical downward force and moment about the ship's transverse axis, leading to an increase in sinkage, trim and resistance.

The three main parameters influencing ship squat are the blockage factor (S), the block coefficient (C_B), and the ship's velocity (V). The blockage factor can be defined as the ratio of the submerged midship cross-sectional area and the underwater area of the canal or channel (Fig. 1). This dimensionless parameter is utilised in calculating ship squat by empirical formulations, and is shown in Eq. (1):

$$S = \frac{bT}{BH} \quad (1)$$

where b is the ship's beam, T is the even keel draught, B is the breadth of the canal or channel and H is the depth. For horizontally unrestricted shallow waters, the effective canal width is used. The effective canal width depends on the ship's waterplane coefficient (C_W) and beam (b) as shown in (31) in the appendix. For the configuration to be defined as unrestricted, most researchers have required S to be equal to or smaller than 0.05 (Briggs, 2006). Underkeel clearance (UKC) and depth Froude number are also other parameters have an influence of ship squat as discussed in the following sections.

In recent years, a rapid increase in ship size has been observed (Debaillon, 2010). This has caused interest in the squat phenomenon and the hydrodynamic behaviour of large ships in confined waters. For instance, supertankers (Ultra Large Crude Carriers, ULCCs) of displacement larger than 300 000 DWT are not uncommon nowadays. This notable increase in size has also been coupled with a gradual increase in operational speeds from 16 to 25 knots, for example, this is valid for some containerships (Tezdogan et al., 2016). For the purpose of ensuring safe navigation and to avoid groundings in shallow waters, for instance when visiting ports, entering rivers or canals, accurate and reliable squat prediction tools are of paramount importance.

As interest in the field of shallow water hydrodynamics of large vessels has increased, the Permanent Association of Navigation Congress (PIANC, 1997) formed a working group (WG 30) to investigate the performance and behaviour of ships in restricted waters. More specifically, WG 30 was tasked with providing recommendations for the design of channels that can accommodate the safe handling of large ships. This includes, but is not limited to, the alignment, width and depth of the channels, and port entrances, and the size of manoeuvring spaces within the channel with special reference to stopping and swinging areas. To do this, WG 30 compiled a list of empirical formulations from different authors. Some of these formulae have been derived based on model experiments and full scale observations, such as the formulation proposed by Barrass (1981). According to Demirbilek and Sargent (1999), values calculated by the distinct formulations may differ by an unacceptable amount for the same input parameters.

In order to accurately assess the ship's power requirements, it is important to understand the resistance a vessel would encounter throughout its operational life. As a consequence of the hydrodynamic interaction between the vessel and the seabed, a significant increase in resistance arises. According to some authors, ships experience a drop in speed of up to 30% upon entering shallow waters (Tezdogan et al., 2016). This value can rise up to 60% when operating in rivers or canals (Barrass, 2012). Such a dramatic speed reduction is directly attributable to the increase in resistance and the change in manoeuvring characteristics. Beck et al. (1975) investigated both a channel with the presence of a depth discontinuity (dredged channel) and a vertical-walled canal. They found that the water surrounding the depth discontinuity in a dredged canal configuration can affect the computed results significantly.

Many port authorities carry out continuous bottom surveys and maintenance dredging to accommodate the limited underkeel clearance of modern ships. A clear international tendency of increase in containership size can be observed,

mainly because of the ‘economies of scale’ which are induced in this way (Gourlay et al., 2015). Furthermore, larger ships are more efficient, which is one of the approaches of conforming to the International Maritime Association’s (IMO) fuel efficiency regulations (Wang et al., 2014). Some of these new vessels have dimensions of 400 m in length, 58 metres beam and 16.5 metres draught, which have already caused several ports to undergo dredging projects (Gourlay et al., 2015). A better understanding of the dynamic squat phenomenon can significantly reduce the adaptation costs of harbours to accommodate the new super ships. Furthermore, a better grasp of the risk involved in shallow water operations for big ships has the potential to reduce the operational costs for all parties involved.

In order to allow vessels to avoid the uncertainty involved in shallow water operations coupled with severe sea states, Norway has commissioned the Stad Ship Tunnel (Perry, 2017). This would allow ships to safely move from one side of the Stadlandet peninsula to the other, without the need of being exposed to the adverse conditions frequently present around the landmass. The nature of the tunnel will be highly restrictive in terms of width and depth, making confined shallow water behaviour and performance prediction highly relevant.

The literature offers a wealth of techniques to calculate the squat and trim of a ship in restricted waterways. These include empirical formulations, analytical, experimental and numerical methods. The empirical formulations can give substantially different values when applied to the same case-study. Furthermore, different parameter restrictions are imposed by each formula, which further complicates their use. Analytical methods use slender-body theory and the assumptions inherent of this approach. Experimental methods can be expensive and highly dependent on the schedule and availability of testing facilities. On the other hand, computational fluid dynamics (CFD) techniques have been shown to be capable of accurately predicting the sinkage, trim and resistance of vessels in shallow waters. Moreover, this can be done while accounting for viscous effects as well as non-linear terms.

For the abovementioned reasons, the current study aims to conduct an in-depth parametric analysis and prediction of the resistance, trim and sinkage of a vessel advancing through a channel with varying underwater topographies. In this respect, the Slenderflow code is used in this study. The code has been devised employing the Slender-Body theory developed by Tuck (1966) for shallow open water, Tuck (1967) for canals, and later expounded upon by Beck et al. (1975) to incorporate dredged channels. The empirical formulations compiled by PIANC (1997) and Briggs (2006, 2009), are also coded into a separate MATLAB code for comparison. A commercial CFD package was utilised to carry out unsteady Reynolds Averaged Navier-Stokes (RANS) simulations on the Duisburg Test Case (DTC) containership for varying speeds and channel geometries. For each simulation, the trim, and sinkage time-histories were recorded at the vessels centre of gravity (CoG) as well as the drag shear and pressure forces time-history. For the purposes of this study, Star-CCM+, version 11.02, developed by CD-Adapco was used. In addition, the supercomputer facilities at the University of Strathclyde were made use of, to allow much faster and more complex simulations to be performed.

The novelty of this study lies in the methods utilised and parameters evaluated. To elaborate, the literature review in Section 2 reveals that no similar study exists, incorporating dredged channels using a CFD technique.

This paper is organised as follows: Section 2 gives a brief literature review on the squat evaluation techniques. A subsection is dedicated to the background required to enable a better understanding of the analytical theory used. Section 3 outlines the rationale behind the ship channel case-study selection. Next, Section 4 is devoted to the CFD numerical modelling, separated into sub-sections delineating the relevant information and decision-making. The results obtained are presented in Section 5, which is split into sub-sections, each concerning a different aspect of the data computed. Finally, concluding remarks and suggestions for future work are given in Section 6.

2. Background

This section is organised in accordance to the squat evaluation methods. To elaborate, the first part is concerned with what seems the most basic way of assessing the ship behaviour and performance in shallow waters, namely, via empirical formulations. Background on the analytical method employed in this paper is then given. A sub-section is provided to detail the rationale behind the equation and boundary condition selection for this method. Finally, the CFD numerical technique used is put into historical perspective.

2.1. Empirical methods

The formulation developed by Eryuzlu and Haussler (1978) was derived based on model-scale experiments carried out on three self-propelled Very Large Crude Carrier (VLCC) models. The full scale-equivalent of which constitutes 227 000 DWT or less. From the experiments, a relationship between the sinkage, velocity and draught was found. An alternative formulation was proposed by the International Commission for the Reception of Large Ships- ICORELS (1980). A joint financed project with PIANC led to the creation of working group 4 (WG 4), which was tasked with providing recommendations for the optimal layout and dimensions of large ships in shallow waterways. More specifically, WG 4 focused their efforts on the North Sea, the Baltic Sea, the Straits of Dover and the Straits of Malacca. Although some recommendations are given regarding the dimensions of dredged canals and navigational aids, the report’s overall conclusion is that “it is not possible to state a general rule for minimum underkeel clearance and manoeuvring areas, because of the influence of local conditions, currents and swell”.

Barrass (1981) proposed a formulation based on model-scale experimental data and full-scale observations. His formula has been improved and updated several times between 1981 and 2006. Römisch et al. (1981) developed the only formula,

Table 1

Empirical formulae constraints, adopted from Briggs (2006).

Formula	Constraints				Configuration		
	C_b	h/T	L/h	F_d	U	R	C
Barrass (1981)	0.5 to 0.9	1.1 to 1.5			✓	✓	✓
Eryuzlu and Hausser (1978)	≥ 0.8	1.08 to 2.75			✓	✓	
Eryuzlu and Hausser (1978)	≥ 0.8				✓		
Hooft (1974)					✓		
ICORELS (1980)					✓		
Millward (1990)	0.44 to 0.83		6 to 12		✓		
Millward (1992)			6 to 12		✓		
Norrbin (1986)					✓		
Römisch et al. (1981)		1.19 to 2.25			✓	✓	✓
Ankudinov et al. (1996)				≤ 0.6	✓	✓	✓
Yoshimura (1988); Ohtsu et al. (2006)					✓	✓	✓

* Trim, midship sinkage coefficient and squat.

other than the (Ankudinov et al., 1996), formulation, capable of calculating the stern squat as well as bow squat of a vessel, which was developed based on model-scale experiments. Later, Millward (1990) proposed a solution, partly as a response to the grounding of the ferry Herald of Free Enterprise (Millward, 1990). The formulas suggested in their paper are intended to be used as an aid in preliminary design calculations and were derived by analysing available experimental data. Later, in Millward (1992) the formulation was re-arranged to resemble the one proposed by Tuck (1966). Following this, Eryuzlu et al. (1994) collected physical full-scale data and conducted model-scale tests on bulk carriers and cargo ships with bulbous bows in restricted and unrestricted waterways. Their investigation led to the development of a formula, which has one restriction less than the (Eryuzlu and Hausser, 1978) formulation. Namely, the validity of the formulae is not governed by the water depth.

To facilitate the comparison of the output from the different formulae detailed above, an in-house code was developed in this study. For this purpose, MATLAB was utilised due to the wealth of complex built-in, easy to understand and use mathematical operators. The formulae coded, and their restrictions are shown in Table 1, where U stands for horizontally unrestricted waters, R represents dredged/restricted channels and C – vertical walled canals:

2.2. Analytical methods

Interest in the field of shallow water hydrodynamics can be traced back to the famous paper by Michell (1898). In his publication, he devised a thin-body method to predict the wave resistance of a ship moving in shallow water. The fundamental assumption behind the Michell (1898) method is that the ship's beam is small compared to its length. As a consequence of this, the waves generated are also of small amplitude, which allows the linearisation of the free water surface. Later Joukovski (1903) derived a similar formulation of the problem independently.

Havelock (1908) investigated the wave pattern created by the propagation of a point source in shallow water. His work led to the introduction of the non-dimensional depth Froude number (F_d)

$$F_d = \frac{V}{\sqrt{gh}} \quad (2)$$

Where V is the vessel's speed, g is the acceleration due to gravity ($g = 9.81 \text{ m/s}^2$) and h is the water depth. The depth Froude number can be thought of as the ratio of the ship's speed to the maximum wave velocity in shallow water of depth h . The well-known Kelvin wave pattern resulting from moving objects in water can be observed at $F_d < 0.57$ (Tezdogan et al., 2015). As the ship's velocity increases, the lateral wave lengths will increase until F_d becomes 1, which is called the critical speed. The terms subcritical and supercritical speed are used for vessels propagating at $F_d < 1$ and $F_d > 1$, respectively. Of greater practical interest is the former scenario, namely when the depth Froude number is smaller than 1 (Beck et al., 1975).

A critical paper, which can be said to have spiked the interest in shallow water hydrodynamics, was produced by Kreitner (1934), who used a one-dimensional hydraulic theory to calculate ship squat. He showed that the equation for the flow velocity in a canal ceases to provide rational solutions as the critical speed is approached. This theoretical prediction made has been extensively verified. It is well known from the work of Constantine (1960), who investigated the relationship between subcritical, critical and supercritical speed regimes and their effect on squat, that laterally restricted waterways have substantial effect on the dynamic squat of a vessel.

The wave-making resistance of ships in shallow seas and restricted waters was investigated by Inui (1954). The abovementioned work showed that the wave-resistance of a ship in infinitely wide shallow water has a continuous character throughout the speed range. However, this does not hold for the first derivative of the resistance with respect to the velocity. On the other hand, the resistance itself is not a continuous function of F_d in the case of restricted shallow waters. Inui (1954) concluded that increasing the restrictions of a waterway, causes higher degrees of discontinuity in the wave-resistance of a ship as a function of F_d .

[Tuck \(1966\)](#) reproduced Michell's linearised Slender-body theory, using matched asymptotic expansions to solve for the hydrodynamic forces in shallow water. In his paper, [Tuck \(1966\)](#) explored the scenario where a ship is travelling in shallow waters of constant infinite width. He used the vertical forces and moments acting on the ship to successfully compute the sinkage and trim for sub- and supercritical speeds, and validated the results with model-scale experiments. The results obtained showed good agreement with experimental results for $F_d < 0.7$ ([Tuck, 1966](#)). One of the main conclusions drawn in his study was that although the theory fails as $F_d \rightarrow 1$ because the formulations used become singular, sinkage is predominant in the subcritical range, while trim is the leading factor in the supercritical range. With regards to resistance, the method developed by [Tuck \(1966\)](#) predicts zero resistance in the subcritical range. [Tuck \(1966\)](#) postulates that if a second order approximation is sought, non-zero resistance in the subcritical range would be achieved as a consequence of the introduction of additional finite-depth effects.

Later, [Tuck \(1967\)](#) investigated the effect of restricted channel width as well as depth on ship behaviour. [Beck et al. \(1975\)](#) expanded on the previously mentioned work to account for vessels in dredged canals ([Fig. 2](#)) with an infinite shallow water region of constant depth (h_∞) extending on either side of the dredged section on the channel (of depth h_0).

As reported in [Gourlay \(2008\)](#), the theory described above is best suited for long, slender hulls such as high speed twin hull catamarans, frigates and destroyers. However, the Slender-Body theory has been successfully implemented on containership hulls whose beam (B) to length (L) ratio lies between 0.11 and 0.15. It is worth noting that the post-panamax containership (DTC) studied in this paper has a ratio $B/L \approx 0.14$, which falls within the restriction detailed above.

[Yasukawa \(1993\)](#) presented a linearised method capable of calculating the wave-making resistance of a ship while taking into account the sinkage and trim based on double-body flow solutions. His approach was applied to the Wigley hull, and showed satisfactory predictions when compared to experimental data. Later, all linearised slender-body methods were compiled and presented in [Gourlay \(2008\)](#). He derived a general Fourier transform method to calculate the sinkage and trim of a ship advancing in unrestricted shallow waters, canals and stepped channels as well as channels of arbitrary cross-section. The formulations [Gourlay \(2008\)](#) used in his paper focus exclusively on the subcritical range of motion. Later, he extended his modification of the Slender-body theory to calculate the sinkage and trim of a fast displacement catamaran propagating through horizontally unrestricted shallow water, which retains its validity for all speed regimes. Then, [Gourlay \(2008\)](#) went on to show how trim, resistance and sinkage are affected by a change in the spacing between the catamaran hulls. Although this method has not been verified against experimental results, [Gourlay \(2008\)](#) postulates that his theory could be used as a preliminary assessment of the sinkage a fast displacement catamaran will experience upon entering shallow waters.

[Alderf et al. \(2011\)](#) suggested the use of a finite element technique to assess the dynamic squat phenomenon. The model developed in their paper was used to validate the stability model as an extension of the method proposed by [Janssen and Schijf \(1953\)](#) by predicting the unstable squat positions for a vessel. Following this, [Yao and Zou \(2010\)](#) developed and tested their theory for a Series 60 hull ($C_B = 0.6$). The approach used in their paper consists of a panel method, applied to calculate the shallow water effects on a ship by discretising the hull, free and wall surfaces into panels on which Rankine sources of constant strength are distributed. The results obtained, which include sinkage, trim, resistance and wave patterns were calculated for sub- and supercritical speeds. The data was found to be in good agreement with experimental results.

Then, [Alidadi and Calisal \(2011\)](#) conducted a numerical study to predict the squat of the Wigley hull. A slender-body theory approach was utilised to convert the three-dimensional ship problem into a series of 2-D cross sections distributed from the bow to the stern at equal intervals. They applied a boundary element method sequentially to each cross section to obtain the disturbance potential. By integrating the pressure over the hull, the forces acting on the hull were derived, which were then used to estimate the squat. A validation study was performed which compared the numerical results with those recorded from experiments at several speeds. The results between the two sets of data were agreeable.

[Gourlay et al. \(2015\)](#) performed a dynamic sinkage and trim comparison and analysis using the Slender-Body theory and Rankine-source method for different modern containership hull forms, including the DTC. The results were compared with experimental data for all case-studies. The key findings are that the Slender-Body theory provides good approximations when applied to wide canals or open water. However, it under predicts the sinkage in narrow canals. With regards to trim, [Gourlay et al. \(2015\)](#) showed that this parameter is accurately assessed for low speeds. The Rankine-source theory showed best performance when applied to the KCS, where the sinkage was similar to experimental results.

Finally, [Feng et al. \(2016\)](#) developed a Rankine source method which utilises the continuous distribution of source panels along the free and seabed surfaces. In this way, no desingularisation was required, which facilitated the investigation performed by [Feng et al. \(2016\)](#) into the performance characteristics of a 2-D structure experiencing a forced oscillation, by removing any additional assumptions. To show the effect the proximity and topology of the seabed, several scenarios were investigated in their research article, including a deep water case-study, flat bottom shallow water, and various uneven bottom topologies. One of the key findings made by [Feng et al. \(2016\)](#) was that the mean water depth is a key parameter influencing the hydrodynamic performance of a body in shallow water.

2.2.1. Slender-Body theory

In this sub-section, the basis of the Slender-Body theory background is given. As a case-study the channels utilised by [Beck et al. \(1975\)](#) to derive their extension to the Slender-Body theory were used in this paper. The same notation used by [Beck et al. \(1975\)](#) is adopted to alleviate the nomenclature and results comparison. The basic concept is shown in [Fig. 2](#):

In [Fig. 2](#), the origin is placed and fixed amidships and coincident with the ship centreline (y -positive to starboard). The vessel is assumed to be stationary, while the fluid moves in the positive x direction. The z -axis, positive upwards, is positioned at the mean surface.

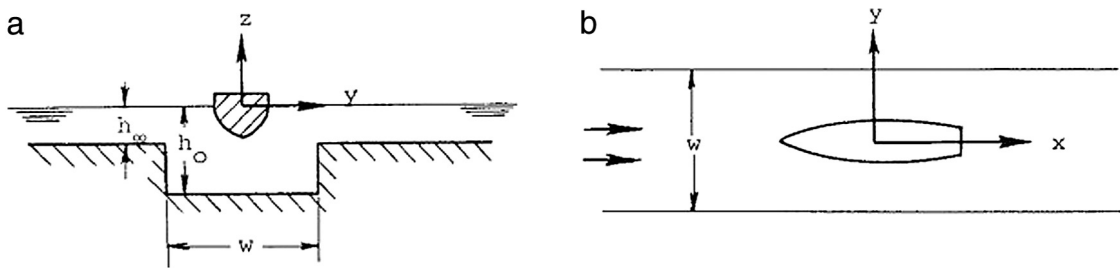


Fig. 2. Schematic drawing of a ship in dredged canal; a: Front view, b: Top view (Beck et al., 1975).

A crucial part of any physics modelling problem lies in the boundary conditions. For the dredged canal, the fluid velocity disturbance due to the presence of a vessel satisfies Laplace's equation in both the interior and exterior regions. Ignoring the local behaviour of the fluid near the hull, the three-dimensional velocity potential can be reduced to 2-dimensions. Therefore, Laplace's equation for the interior/exterior region takes the form of:

$$(1 - F_d^2) \frac{\partial^2 \varphi}{\partial x^2} + \frac{\partial^2 \varphi}{\partial y^2} = 0 \quad (3)$$

Where φ is used to denote the velocity potential. For $F_d < 1$, the solutions of Eq. (3) approximate an elliptical function; while for $F_d > 1$ the solutions show a hyperbolic tendency. This paper will only deal with the cases where the solutions of Eq. (3) are elliptical, or in other words, the flow lies in the subcritical range. Then, Tuck (1966) goes on to describe the hull boundary condition, namely, the velocity normal to the hull is equal to zero:

$$\frac{\partial(x + \varphi)}{\partial n} = 0 \quad (4)$$

where $\partial/\partial n$ is the derivative in the normal direction. Furthermore, the same boundary condition holds for the bottom of the channel $\frac{\partial \varphi}{\partial z} = 0$.

Utilising the results derived by Tuck (1966), it follows from the mass conservation law that the velocity potential must satisfy the boundary condition, Eq. (5) (Gourlay, 2008):

$$\frac{\partial \varphi}{\partial y} = \pm \frac{V}{2h_0} S'(x) \text{ at } y = 0 \text{ i.e. at the hull} \quad (5)$$

where $S(x)$ is the hull cross-sectional area at position x , and prime is used to denote the derivative $\frac{ds}{dx}$, h_0 is the interior water region depth, and V is the ship speed.

The second boundary condition contains two parts. Firstly, for a fluid extending infinitely in the y direction, the potential $\varphi \rightarrow 0$ as $y \rightarrow \pm\infty$ for $F_d < 1$. Secondly, $\varphi \rightarrow 0$ as $x \rightarrow \pm\infty$.

The bottom topography is described in the same terms as by Beck et al. (1975), to elaborate, the fluid extends throughout the region $-h(y) < z < 0$, where $h(y)$ can be described in terms of the interior region's width as shown in Eq. (6):

$$h(y) \begin{cases} h_0, & |y| < w/2 \\ h_\infty, & |y| > w/2 \end{cases} \quad (6)$$

Eq. (6), implies that the location of the hull's centreline and coordinate system coincide with the channel's. Additionally, the domain, occupied by the fluid can be separated in terms of two depth Froude numbers $F_\infty = V/\sqrt{gh_\infty}$ which corresponds to the exterior region and $F_0 = V/\sqrt{gh_0}$, which corresponds to the interior region. In the paper by Beck et al. (1975), the flow in the interior region is always taken to be subcritical ($F_0 < 1$). Therefore, the cases investigated are reduced to:

1. The exterior region is subcritical ($F_\infty < 1$) – the sub-sub case
2. The exterior region is supercritical ($F_\infty > 1$) – the sub-super case

In both the studies of Beck et al. (1975) and Tuck (1966), the boundary condition, Eq. (5) is integrated by parts and the hull cross-sectional area is assumed to equal zero at the bow and stern. However, firstly, this assumption does not hold for modern transom ships (Gourlay, 2008). Secondly, for certain speeds, the flow cannot close immediately after the transom i.e. there is some flow separation in the stern section of the ship. Therefore, Gourlay (2008) proposed that the gradient of the sectional area should be taken as 0 ahead of and behind the vessel, instead. This allows for the boundary condition Eq. (5) to be used in its original form. Gourlay (2008) then employed the direct Fourier transform of the derivative of the cross-sectional area over the wetted length of the ship:

$$\bar{S}'(k) = \int_{-\infty}^{\infty} S'(x) e^{ikx} dx \quad (7)$$

According to Gourlay (2008) this ensures the smooth detachment of the flow from the transom even at high speeds. Furthermore, in the abovementioned article, the author argues that the assumption of a ‘bang shut’ flow, i.e. no flow separation, behind the transom makes the derived theory less applicable to modern ships.

For stepped channels, Beck et al. (1975) proposed two methods for calculating the force and moment coefficients and therefore the sinkage and trim. The first method uses the Fourier transform of the ship’s beam ($b(k)$) and the beam multiplied by the position ($xb(k)$). The alternative method utilises the convolution of the derivative of the cross-sectional area and the dimensionless parameter $k(x)$, mathematically defined as shown in Eq. (8):

$$k(x) = \left[\coth \frac{\pi x}{w\sqrt{1-F_0^2}} - 1 \right] \exp \left(\frac{2\theta w}{w\sqrt{1-F_0^2}} \right) \quad (8)$$

Where

$$\theta = \begin{cases} \arctan \left(\frac{h_\infty \sqrt{F_\infty^2 - 1}}{h_0 \sqrt{1 - F_0^2}} \right) & \text{for } F_\infty < 1 \\ i \operatorname{sgn}(k) \arctan \left(\frac{h_\infty \sqrt{1 - F_\infty^2}}{h_0 \sqrt{1 - F_0^2}} \right) & \text{for } F_\infty > 1 \end{cases} \quad (9)$$

where $i = \sqrt{-1}$ and $\operatorname{sgn}(k)$ is the signum of the Fourier transform variable k .

Making use of the convolution method described by Beck et al. (1975), the resulting equations for the force and moment coefficients (C_f and C_m respectively):

$$C_m = \frac{\int xb(x) \int s'(\xi) k(x - \xi) d\xi dx}{2wL\sqrt{1 - F_0^2} \int b(x) x^2 dx} \quad (10)$$

$$C_f = \frac{\int b(x) \int s'(\xi) k(x - \xi) d\xi dx}{2wL\sqrt{1 - F_0^2} \int b(x) dx} \quad (11)$$

where $\int s'(\xi) k(x - \xi) d\xi dx$ is the convolution mentioned previously, \int is used to denote the Cauchy or principle value integral and ξ is the convolution variable.

Eqs. (10) and (11), respectively, are used to calculate the sinkage and trim coefficients – Eqs. (12) and (13), respectively:

$$C_s = \frac{C_f - \alpha C_m}{1 - \alpha \beta} \quad (12)$$

$$C_\vartheta = \frac{C_m - \beta C_f}{1 - \alpha \beta} \quad (13)$$

where the shape parameters α and β are defined in Eqs. (14) and (15):

$$\alpha = \frac{\int xb(x) dx}{L \int b(x) x^2 dx} \quad (14)$$

$$\beta = \frac{L \int b(x) x dx}{\int b(x) x^2 dx} \quad (15)$$

An interesting property that Eq. (14) to (15) exhibit is that they all vanish for a longitudinally (y -axis) symmetrical ship (Tuck, 1966). The explanation to this lies in the integration of the beam over the length, multiplied by the position function in Eqs. (14) and (15). For such a ship, the coefficients α and β must equal zero due to the integral in the numerator. Similarly, in Eq. (10) integrating the beam over the length when $b(x)$ is a symmetrical curve yields zero.

The expressions for the sinkage (Eq. (16)) and trim (Eq. (17)) proposed by (Tuck, 1966) retain their validity in Beck et al. (1975). To elaborate,

$$s = \frac{LC_s F_0^2}{\sqrt{1 - F_0^2}} [\text{m}] \quad (16)$$

$$t = \frac{C_\vartheta F_0^2}{\sqrt{1 - F_0^2}} [\text{radians}] \quad (17)$$

The only change necessary to obtain a formulation for a ship advancing through a canal with vertical walls on either side or $h_\infty/h_0 = 1$ and no infinite shallow water region, lies in the parameter θ . As the ratio of the shallow water region to the deep water region is part of the argument of the inverse tangent of θ , the parameter $\theta \rightarrow 0$ for such a scenario. Therefore, no difficulty arises in computing the coefficients of interest for different channel geometries. One of the key conclusions drawn by Beck et al. (1975) is that as h_∞ diminishes, the wave resistance increases. It is important to note that these results have yet to be validated. The current study incorporates several case-studies designed to investigate further into this prediction.

An immediate inference drawn from this section is that most authors employ directly the Slender-Body theory, such as Gourlay et al. (2015), Gourlay (2007), (2008), (2009) and Alidadi and Calisal (2011). Alternatively, similar linearised methods are utilised in the literature to solve the problem of dynamic squat-induced sinkage, trim and resistance. One of the major shortcomings of these approaches is that the non-linear terms are neglected. Gourlay (2008) stated that these higher-order terms do not significantly affect the performance of slender bodies propagating in shallow waters. However, the behaviour of larger vessels that operate at relatively high speeds, such as containerships and car carriers, can be significantly influenced by this assumption.

2.3. Reynolds Averaged Navier–Stokes (RANS) based numerical techniques

In this section, the Computational Fluid Dynamics (CFD) contribution to the field of shallow water hydrodynamics is delineated. Unlike potential flow theories, CFD has not yet been used extensively to predict the sinkage, trim and resistance of ships in shallow waters. For instance, Jachowski (2008) employed a commercially available RANS based numerical software package to predict ship squat in shallow waters. He applied this technique to the KRISO Containership (KCS) model. In order to reduce the computational effort, all simulations performed in his paper were carried out in model scale. Additionally, a symmetry boundary condition was imposed due to the transverse symmetry of the flow around the hull (Jachowski, 2008). The results were compared to those calculated by empirical formulations and good agreement was found between the two methods.

Later, Prakash and Chandra (2013) performed a CFD analysis of a ship advancing through shallow waters using ANSYS Fluent, a commercial RANS solver. Their paper consists of an investigation into the resistance of a river-sea ship at different speeds. The CFD based software was run in deep and shallow water, in model scale for different speeds, 5 of which in the subcritical, one critical and one in the supercritical range (Prakash and Chandra, 2013). The data obtained by CFD was then compared to the Holtrop (1978) method for the deep water case. The method developed by Schlichting, an empirical approach estimating the proportional increase in resistance when comparing deep and shallow water performance, was used by Prakash and Chandra (2013) to validate the shallow water results (Lewis, 1988).

Wortley (2013) performed a CFD investigation of the sinkage and trim on the DTC containership in OpenFOAM, an alternative RANS solver. Wortley (2013) used two different software packages (Maxsurf and Michlet) to compare his results. Wortley (2013) reported that as a consequence of the insufficient resolution of the generated mesh in OpenFOAM, the wave resistance is overestimated. Furthermore, the sinkage and trim results obtained showed some disagreement with experimental results. As reported by Tezdogan et al. (2016), provided that the CFD setup is refined, the results will agree well with the values obtained experimentally.

Castiglione et al. (2014) performed a numerical study on the interference effects of wave systems on a catamaran in shallow water. Their investigation was conducted using the CFDShip-Iowa RANS solver on the DELFT 372 catamaran model. As part of their study, two hull separation distances and three depth scenarios were computed for several speeds. Some of their key findings are that ship-generated waves and their interference change significantly and are more relevant in shallow, rather than deep water. Furthermore, shallow waters have a significant effect on the total resistance of a ship. To evaluate the multi-hull performance of the catamaran, Castiglione et al. (2014) extended their research by incorporating mono-hull case-studies as well.

Mucha and El-Mohtar (2014) performed numerical analyses using potential flow and RANS methods and compared their results for sinkage, trim and resistance to available experimental data for the KCS model in shallow water. The resistance was predicted well by the RANS solver, while the potential flow method showed small deviations from experiments. One of the interesting findings from their study is that the frictional resistance of a ship is highly dependent on the underwater keel clearance (UKC). The results for sinkage and trim were also in good agreement with the available data. The RANS solver showed some deviation from the experimental data in the low speed range, which the authors attribute to reduced quality of the grid on the free surface. Finally, the authors concluded that there is a need for further systematic investigation into shallow water effects.

More recently, Tezdogan et al. (2016) investigated the performance and behaviour of the DTC in an asymmetric canal as part of the Pre-Squat workshop initiated by the University of Duisburg–Essen (further information can be found in (Mucha et al., 2014)). Simulations were run for different even keel draughts and speeds to evaluate the effect of the asymmetric bottom on the channel. To accomplish this, Tezdogan et al. (2016) employed CD-Adapco's Star-CCM+ RANS solver and showed that the results obtained in model scale are in good agreement with experimental results. Perhaps one of the most interesting findings was that a slightly increased large initial draught will magnify the effect of the shallow water region to a much greater extent than a significantly increased small initial draught (Tezdogan et al., 2016).

In this paper, the same vessel as the one used by Tezdogan et al. (2016) is used and the numerical setup is the same except the canal geometry. In Tezdogan et al. (2016)'s study an asymmetric canal geometry was modelled as adopted from Mucha et al. (2014). Therefore the study reported in this paper heavily relies on the CFD modelling described in Tezdogan et al. (2016), which is already verified and validated against experimental work of Uliczka (2010).



Fig. 3. 3D geometry of the DTC; modelled in Star-CCM+ (Tezdogan et al., 2016).

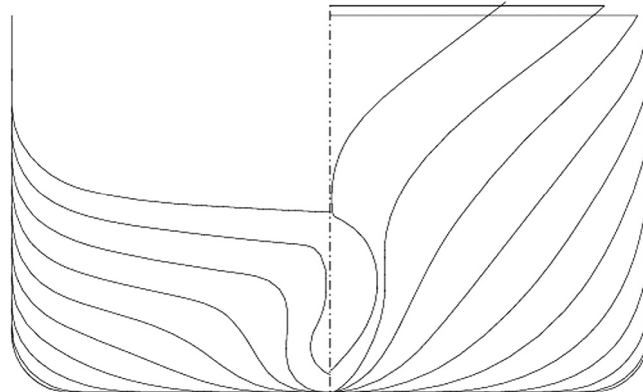


Fig. 4. Hull sections of DTC (El-Mohtar et al., 2012).

Table 2

DTC main particulars in full and model-scale (El-Mohtar et al., 2012).

Property	Unit	Symbol	Full-scale	Model-scale
Length between perpendiculars	m	L	355	8.875
Beam at waterline	m	B	51	1.275
Design draught	m	T	14.5	0.363
Displacement	m^3	∇	173814.762	2.716
Block coefficient	—	C_B	0.661	0.661
Wetted area, including rudder and propeller	m^2	S_W	22352	13.970
Longitudinal centre of Buoyancy	m	LCB	174.531	4.363
Vertical Centre of Gravity – from Keel	m	VCG	23.28	0.852
Metacentric height	m	GM_T	1.677	0.042

3. Ship hull and channel geometry

As a case study for this paper, the DTC model was chosen for several reasons. Firstly, 3-D CAD (Computer-Aided Design) hull, propeller and rudder data are all readily available in the public domain. Secondly, as a response to the rapid developments of containership hull form design, the University of Duisburg-Essen developed this vessel for benchmarking purposes. The DTC was designed to be utilised as a model for numerous investigations, and various authors have made use of the DTC to conduct research (El-Mohtar et al., 2012). A large number of experiments have been carried out in model scale (1 : 40) and a wealth of data is available from different papers in both deep and shallow waters. Unfortunately, a stepped channel model scale experiment is yet to be conducted, which is part of the reason why the present study incorporates this scenario.

For the reasons detailed above, the DTC is the perfect case-study for an investigation into the shallow water behaviour and performance of large vessels. A scale factor of 1:40 was chosen to match the experiments performed on this ship in other studies. A 3D model of the DTC as modelled in Star-CCM+ is shown in Fig. 3 and the hull sections are presented in Fig. 4. As part of the initial conditions, an even-keel draught was set throughout the case-studies performed in this paper. The main particulars in full and model-scale are presented in Table 2.

Since the research idea behind this paper was to investigate the effect of the presence of a step in the channel, it is evident that this scenario will be focused upon. Furthermore, in Beck et al. (1975), great emphasis was placed on the height of the step in proportion to the overall depth. In this study, the abovementioned ratio (h_∞/h_0) was varied between 1 and 0 at three equal intervals for each depth Froude number, as shown in Table 3. To increase the number of ways in which this study can be compared, a suitable channel depth had to be chosen. Although, when carrying out a CFD simulation, there are few vertical restrictions on the domain dimensions, it was decided that the depth should satisfy most of the restrictions imposed by empirical formulations. The majority of the abovementioned formulae require that $1.19 < h_0/T < 1.5$. For this reason, the ratio h_0/T was chosen to equal 1.3, as this is a middle value.

Table 3
Channel configuration.

Case-study	Ratio	Ratio value	Step height (m)
Channel 1	h_∞/h_0	1	0
Channel 2	h_∞/h_0	0.33	0.311
Channel 3	h_∞/h_0	0.66	0.155
Channel 4	h_∞/h_0	0	0.471

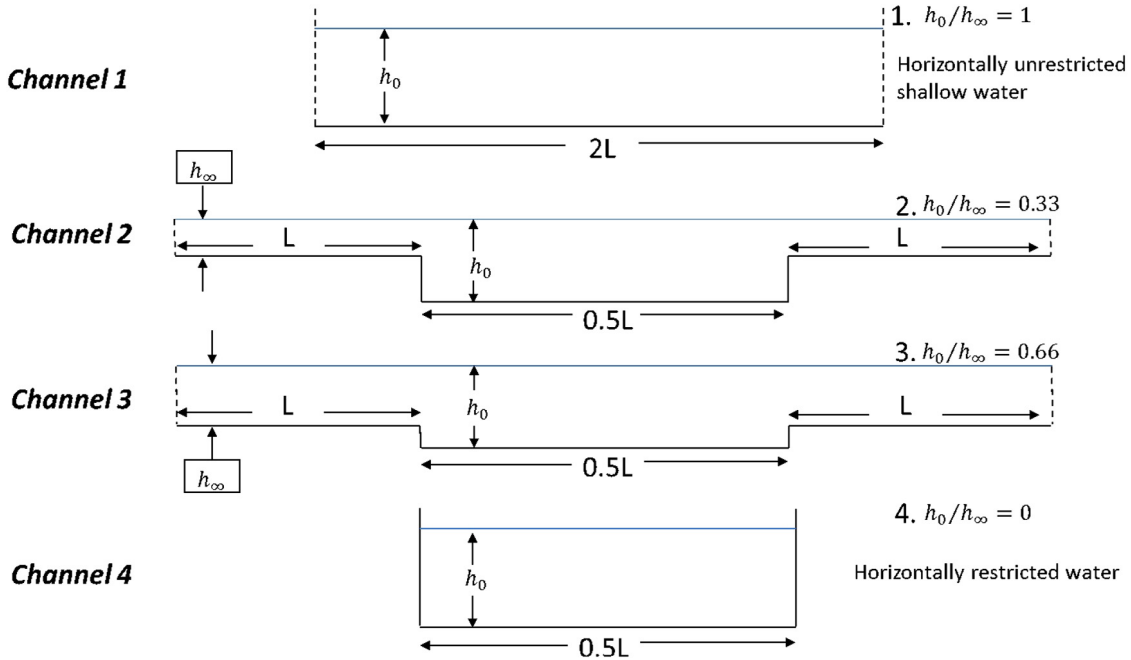


Fig. 5. Channel cross-sections.

The width of the inner region was chosen based on the results detailed by Beck et al. (1975). By reviewing the graphs produced by Beck et al. (1975), it became evident that when the inner width to ship length ratio is equal to 0.5 the effect of the step is amplified. Therefore, this configuration was selected to investigate the influence of the depth discontinuity as this assumption is likely to produce the most palpable differences between configurations. The width of the domain in the research by Beck et al. (1975) is infinite, however, doing this in Star-CCM+, or in fact any CFD software is not possible, therefore, the transverse boundaries must be placed suitably, so that wave reflection does not influence the ship. According to the ITTC's CFD guidelines, any boundary should be placed between 1 and 2 ship lengths away from the vessel (ITTC, 2011). To minimise the computational effort, the lateral boundaries were placed at a distance of 1 ship length away from the step on each side. This amounts to 1.25 ship lengths distance between the vessel's centreline and the transverse boundaries on each side of the ship, as depicted in Fig. 5.

The case-studies detailed in Table 3 are used in both the Slender-Body theory and CFD runs. To compare the performance of these two different methods more accurately, as mentioned in the Introduction, each case-study is run for different speeds. Table 4 shows in detail the model-scale and corresponding full-scale velocity for each run. Additionally, the channel cross-sections are shown in Fig. 5.

4. Numerical modelling

Up to this point, this paper has been focused solely on the motivation and background of the theories and techniques used, and the logic behind the specific case-studies selected. In this section, the numerical modelling techniques will be discussed in detail. As stated previously, the numerical setup employed in this paper is similar to that explained in detail in Tezdogan et al. (2016).

4.1. Physics modelling

Star-CCM+ employs the finite volume method to model the flow, which uses the integral form of the governing equations and divides the computational domain into a finite number of adjoining cells. The RANS solver utilises a predictor–corrector approach to link the continuity and momentum equations.

Table 4

Simulations cases applied to CFD.

Case-study no	Channel	F_0	F_∞	Model-scale velocity (m/s)	Full-scale velocity (kn)
1	1		–		
2	2		0.522		
3	3	0.3	0.369	0.645	7.929
4	4		–		
5	1		–		
6	2		0.696		
7	3	0.4	0.492	0.860	10.571
8	4		–		
9	1		–		
10	2		0.87		
11	3	0.5	0.615	1.075	13.214
12	4		–		
13	1		–		
14	2		1.044		
15	3	0.6	0.739	1.29	15.857
16	4		–		
17	1		–		
18	2		1.219		
19	3	0.7	0.862	1.505	18.5
20	4		–		
21	1		–		
22	2		1.393		
23	3	0.8	0.985	1.72	21.142
24	4		–		
25	1		–		
26	2		1.567		
27	3	0.9	1.112	1.935	23.785
28	4		–		

To model the turbulence in the fluid, a standard $k-\varepsilon$ model was employed with the all y^+ wall treatment, which has been widely used in similar studies Tezdogan et al. (2015, 2016). Quérard et al. (2008) conducted a study in which the viscous effects on ships were investigated. One of their key findings was that the $k-\varepsilon$ turbulence model is inexpensive in terms of CPU usage and can reduce the computational time significantly simultaneously providing solutions in good agreement with available data (ITTC, 2011; Quérard et al., 2008). The model selected here can be described as a two-equation model because it introduces two additional equations for the numerical software to solve, more specifically, one for the kinetic energy (k) and one for the dissipation (ε). Moreover, as stated by CD-ADAPCO (2016), the $k-\varepsilon$ model provides a good compromise between robustness, computational cost and accuracy. As stated in Tezdogan (2015) with a reference to CD-ADAPCO (2016) “the all y^+ wall treatment is a hybrid model, which provides a more realistic approach than the low-Re or the high Re treatments. To calculate shear stress, this well treatment uses blended wall laws, which present a buffer region that suitably blends the laminar and turbulent regions together. The result is similar to the low-Re y^+ treatment as $y^+ \rightarrow 0$ and similar to the high-Re y^+ treatment for y^+ values greater than 30”.

To characterise the free surface, the volume of fluid (VOF) method was adopted to model and position the boundary between phases. This consists of a numerical technique for tracking and locating the fluid–fluid interface (CD-ADAPCO, 2016). The VOF model is defined in the Star-CCM+ user manual as “a simple multiphase model that is well suited to simulating flows of several immiscible fluids on numerical grids capable of resolving the interface between the mixture’s phases” (CD-ADAPCO, 2016). The suitability of this method for predicting the fine changes present in the free surface depends on the two immiscible fluids accounting for large structures in the domain, while their contact area should be relatively small (CD-ADAPCO, 2016). The concept of a flat wave is used to represent the movement of water particles relative to the ship hull in the context of this paper. The water surface is free to move, depending on the disturbance caused by the presence of the ship. An increased mesh resolution is imposed in the region where the free surface is expected to undergo sharp local gradients i.e. the formation of waves. The VOF model has shown excellent performance and high numerical efficiency in similar studies such as ones conducted by Tezdogan et al. (2015, 2016).

The convection terms in the Navier–Stokes equations are discretised using a second order upwind scheme. This was done to avoid the smearing of the free surface, which would likely happen if a lower order scheme had been adopted instead (CD-ADAPCO, 2016).

A segregated flow model was utilised to solve the governing Navier–Stokes equations in an uncoupled manner. To solve these equations, the Semi-Implicit Method for Pressure Linked Equations (SIMPLE) algorithm was utilised.

To ensure the accurate representation of ship motions, Star-CCM+ offers a Dynamic Fluid-Body Interaction (DFBI) module. This allows the user to select which degrees of freedom the structure analysed can move and rotate in. For the purposes of the current study, the DTC was free to trim and sink. The DFBI module simulates the rigid body’s motions in response to shear forces and pressures present in the fluid (ITTC, 2011).

4.2. Time step selection

An important concept for convergence of numerically solved equations is the Convective Courant–Friedrichs–Lowy (CFL) number. The basic concept behind this dimensionless parameter is that if a flow is moving across a discrete spatial grid, its characteristics should be computed at each cell using a predetermined time step (Δt). This must be selected appropriately, so that the time it takes a fluid particle to move from one cell to the next, should be equal to or larger than the chosen value of Δt . Therefore, to ensure that all flow characteristics are captured within the generated grid of cells CFL must be ≤ 1 . The mathematical description of the Courant number is given in Eq. (18):

$$CFL = \frac{u\Delta t}{\Delta x} < 1 \quad (18)$$

where u is the fluid velocity in m/s, Δt is the time step in seconds and Δx represents the length of the control volume or cell in metres. For the case-studies examined here, the Courant number was not kept constant. Instead, the time-step was modified to provide accurate solutions for the flow around the ship over the grid, which was not altered between the case-studies.

To control the time step, the Implicit Unsteady option of Star-CCM+ was selected. An alternative method for time-step selection, proposed by the ITTC (2011) recommends that for resistance predictions, Δt is calculated as shown in Eq. (19):

$$\Delta t = 0.005 \sim 0.01 L/V \quad (19)$$

where L is the length in metres and V is the ship speed in m/s.

In a similar study, where the DTC's sinkage and resistance in shallow waters were analysed, a time-step convergence study was carried out, this suggested that Δt should equal $0.0035L/V$, which is significantly lower than the formulation proposed by the ITTC (Tezdogan et al., 2016). Finally, the temporal discretisation was set as first order to discretise the time variant term in the governing Navier–Stokes equation. This model was selected because it offers a good compromise between accuracy and time required to run the simulation. Additionally, first order temporal discretisation has been shown to provide stable results and good convergence properties in similar studies such Tezdogan et al. (2016). Finally, one of the main advantages of employing first order time discretisation is that the Courant number must be lower than 1, rather than 0.5, which would be required had the alternative (2nd order) scheme been selected.

4.3. Computational domain

In this section, justification behind the computational domain dimension selection is presented. Re-examining the assumptions made by Beck et al. (1975), several guidelines for the domain arise: The width of the domain in Beck et al. (1975) is infinite, however, doing this in Star-CCM+, or in fact in any CFD software is not possible, therefore, the transverse boundaries have been placed suitably.

CD-ADAPCO (2016), recommends that the velocity inlet of the computational domain for resistance prediction should be located at least one ship length upstream from the forward perpendicular, and the pressure outlet at least twice that distance downstream, from the respective perpendicular. The rationale behind this recommendation is that in rare occasions, wave reflection can occur, this can potentially render the results meaningless from a resistance analysis point of view. To conform to these recommendations, the inlet boundary was set $1.22L$ ahead of the forward perpendicular and the pressure outlet $2.23L$ downstream from the aft perpendicular (CD-Adapco, 2016, (Tezdogan et al., 2016)). To eliminate the possibility of a wave reflection from these boundaries, a VOF wave damping option was enforced, the length of which was set as to equal $1.127L \approx 10$ m used in both longitudinal and transverse directions.

There are several types of boundary conditions offered by the CFD software package. For the purposes of this study, only the enforced conditions will be discussed. The boundary in the positive x -direction was set as a velocity inlet, where the flat wave originates, and the negative x -direction was set as pressure outlet, which prevents backflow and fixes static pressure at the outlet. To allow the simulation to resemble real life towing tank experiments as close as possible, the domain top was placed $1.127L \approx 10$ m away from the still waterline, where the Newman boundary condition was applied. This expresses an assumption widely used in potential flow, which can also be useful in CFD modelling. Namely, the velocity normal to the surface is 0 as in Eq. (4). Next, the virtual towing tank bottom is set as a 'wall'- this boundary condition, as defined by Prabhakara and Deshpande (2004), expresses "that a moving fluid in contact with a solid body will not have any velocity relative to the body at the contact surface". Employing the built-in (non-slip) function of Star-CCM+ describing this phenomenon, we have dealt with the domain bottom, sides and hull.

Thus, the computational domain is assembled and shown graphically in Fig. 6 for channel 2.

4.4. Mesh generation

Mesh generation was carried out in the facilities offered by Star-CCM+. This allows the user to make full use of the software's automatic operations. Firstly, the region-based mesh generated is static in relation to the local coordinate system and therefore to the hull. Since the DTC's appendages describe complex geometries (rudder, propeller), a high-quality trimmed cell mesher was utilised, which generated cells in the computational domain, presented in Table 5.

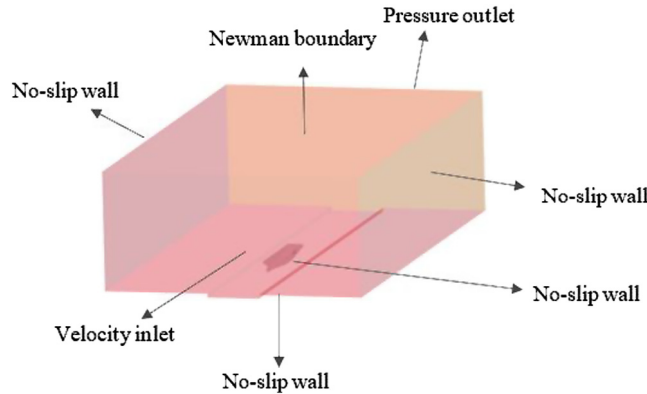


Fig. 6. Representative domain boundaries; Depicted: Channel 2 ($h_\infty/h_0 = 0.33$).

Table 5

The number of cells, faces and vertices for each channel configuration generated by Star-CCM+.

Configuration	Number of cells	Number of faces	Number of vertices
Channel 1	1971465	5894406	2085519
Channel 2	1915989	5721364	2030540
Channel 3	1920352	5734692	2035409
Channel 4	1833069	5465509	1935181

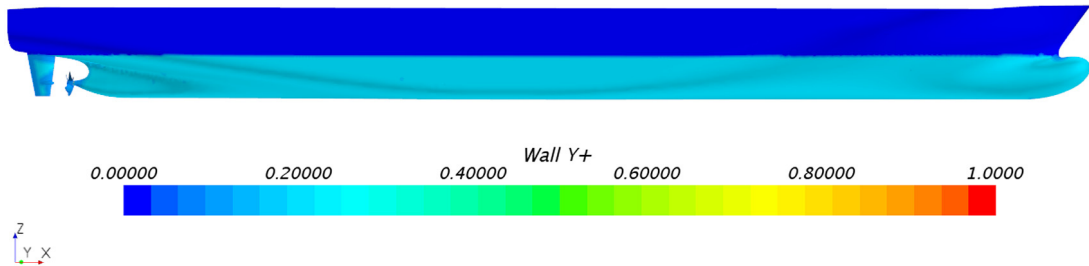


Fig. 7. Wall y^+ distribution on the hull surface.

The Prism Layer mesher was utilised to generate orthogonal prismatic cells next to the hull. This kind of layer mesh allows the software to resolve the near-wall flow accurately as well as capture the effects of flow separation (CD-ADAPCO, 2016). Resolving these parameters in sufficient detail depends on the flow velocity gradients normal to the wall, which are much steeper in the viscous turbulent boundary layer than would be implied by taking gradients from a coarse mesh. Prism layer numbers were selected to ensure that the y^+ value on the ship is maintained at a value lower than 1 in order to use the low-Re y^+ treatment, as explained previously. This was also discussed in the Pre-Squat workshop by Yahfoufi and Deng (2014) as their results claim that accurate calculation of ship squat and resistance relies on the selection of the low-Re model. A graphical representation of the y^+ wall function on the ship hull is given in Fig. 7, where the average value is 0.00878.

A trimmed mesher option was selected, which is an efficient method of fabricating a high-quality grid for complex mesh generation. The cells created by the trimmed mesher are predominantly hexahedral and have a minimal cell skewness. Fig. 8 shows the surface mesh on the hull with a focus on the stern of the ship. The computational mesh has areas refined in size around the hull, rudder and propeller as well as the areas where the free water surface is expected. The wake field behind the vessel also has a refined grid density to capture the complex flow properties (Fig. 9).

4.5. Convergence

An important aspect of any numerical computation is convergence and its time-history. Of particular importance are the deviation amplitudes exhibited by the computed variables as the simulation approaches its end. To ensure a good solution and representation of the results, the values should converge towards some value. As shown in Fig. 10, a typical convergence time-history for the setup used in the present study shows stable computations.

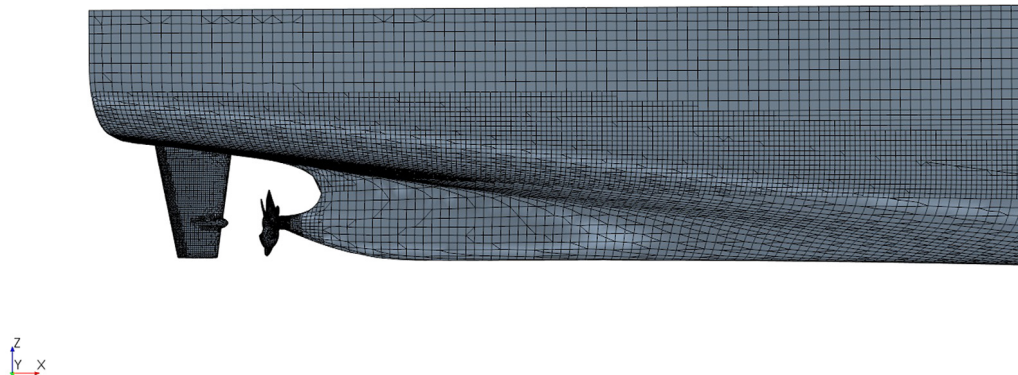


Fig. 8. DTC stern mesh.

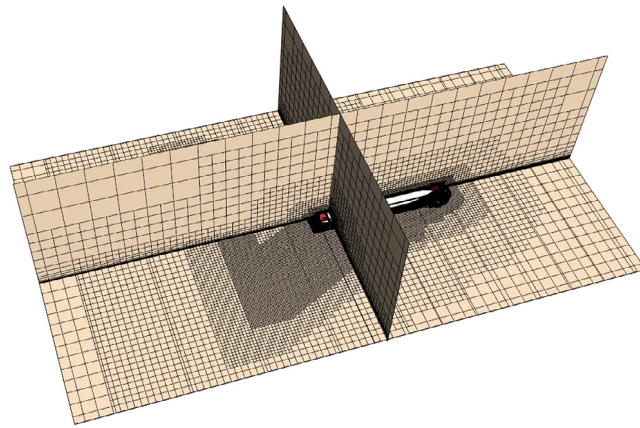


Fig. 9. 3-D view of the mesh. Depicted: Channel 3 ($h_{\infty}/h_0 = 0.66$).

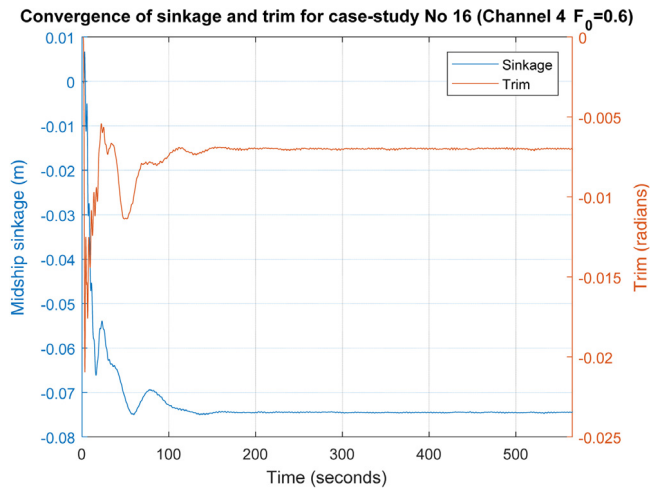


Fig. 10. Convergence time–history of trim and sinkage for case-study No 16.

5. Results and discussion

In this section, the results computed via all different methods are presented and compared. A discussion on the discrepancies discovered is given, in which an attempt is made to explain the disagreements, where present, between the different squat estimation approaches.

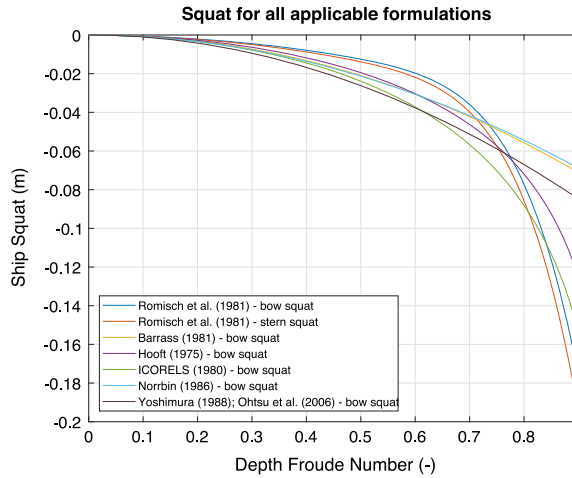


Fig. 11. In-house code output: Empirical formulae for channel 1.

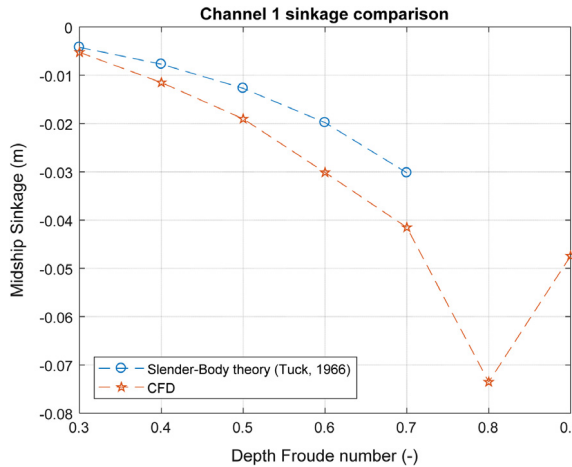


Fig. 12. CFD and Slender-Body theory comparison for channel 1.

To begin with, perhaps the most interesting and most studied variable is analysed, namely, the squat. However, in order to obtain a full picture of the ship behaviour in shallow water, the trim the vessel experiences, considered an indispensable part in the overall ship assessment, is given for each case-study. The trim is given in radians, as the Slender-Body theory output uses this unit. The sinkage coefficients are also presented in this paper to facilitate future work.

5.1. Ship behaviour

5.1.1. Channel 1

For this case-study, an attempt was made to approximate the scenario of a ship advancing through unrestricted shallow water. The theory developed by Tuck (1966) describes this case-study, which has been shown to provide satisfactory results when compared to experimental data for low speeds. To perform the calculations, the Slenderflow code, which is validated in (Ha and Gourlay, *in press*) was used to provide results for all configurations investigated in order to ensure that the results are accurate. The empirical formulations for unrestricted waters were employed in the in-house code. The applicable formulae and the results computed using this method up to $F_d = 0.9$ are shown in Fig. 11.

As discussed previously, Fig. 11 highlights the main issue of this method of calculating ship squat. Namely, the results are highly divergent and disagree significantly, especially in the high-speed range.

To retain consistency, the values computed via the Slender-Body theory and CFD are presented in a together, as both methods calculate the sinkage amidships, rather than at the extremity of the vessel, which can be highly influenced by the trim. The results comparison is shown in Fig. 12.

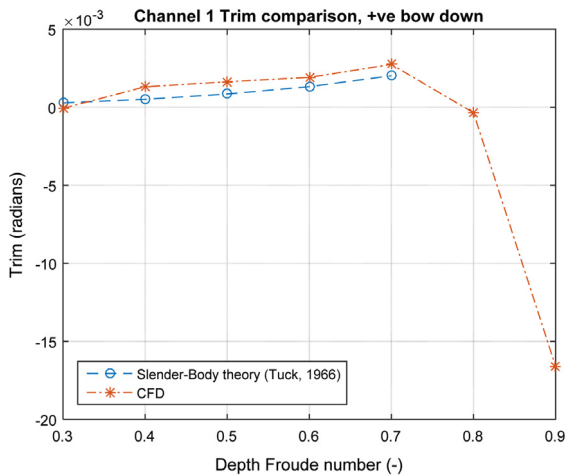


Fig. 13. Dynamic trim comparison for Channel 1; positive bow down.

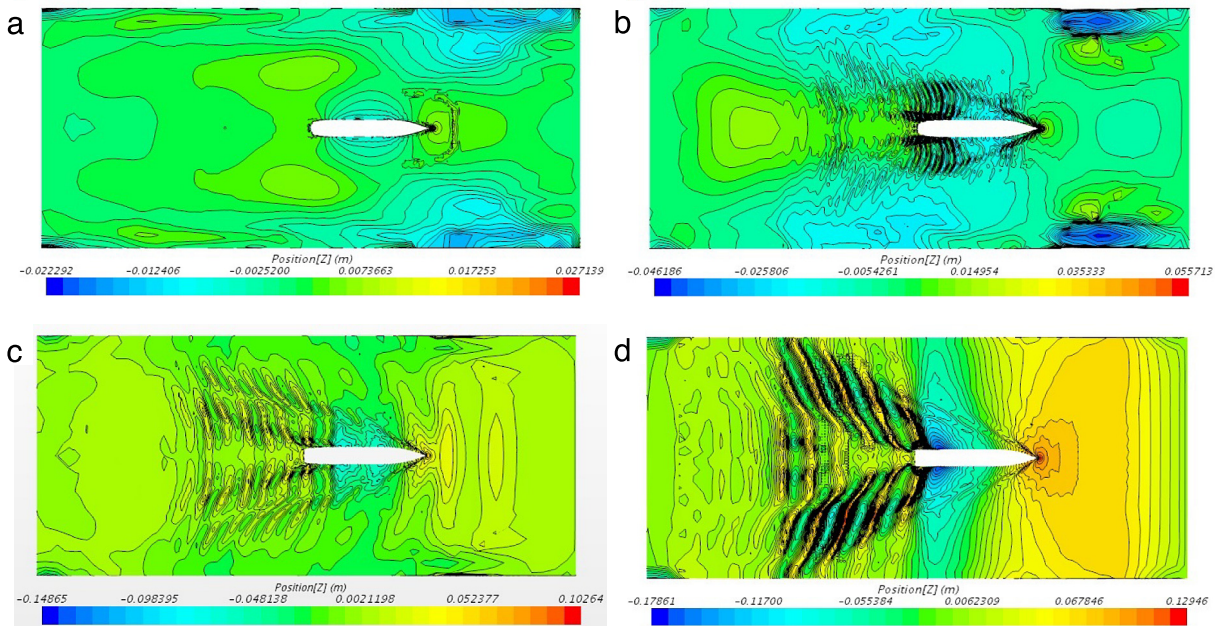


Fig. 14. Wave patterns; Channel 1 at $F_0 = a:0.3, b:0.5, c:0.7, d:0.9$.

The results using the theory developed by Tuck (1966) are continued up to and including $F_0 = 0.7$ because non-linear and viscous effects become more important as we progress through the speed range. A slight underestimation of the CFD results can be observed throughout the velocities investigated, which is a consequence neglect of non-linear and viscous terms (Gourlay, 2008). As expected, the difference between the two sets of data gradually increases as the depth Froude number increases.

Finally, the trim comparison for this case-study is presented. The trim output from the in-house code developed for the empirical formulations is not shown as the results are several orders lower than the Slender-Body theory's prediction or the CFD results.

Fig. 13 reveals results, similar to those obtained by Gourlay et al. (2015). To elaborate, the DTC trims by bow up to $F_0 = 0.7$, which is the upper limit investigated in the abovementioned work. The experimental results for the DTC both in a rectangular and non-rectangular canal, as in Tezdogan et al. (2016), agree that the vessel squats by stern. The novel information presented here is that the DTC rapidly changes the trim mode to stern as the velocity increases past $F_0 = 0.7$.

Finally, the wave patterns for this configuration are given in Fig. 14 for depth Froude numbers 0.3 to 0.9.

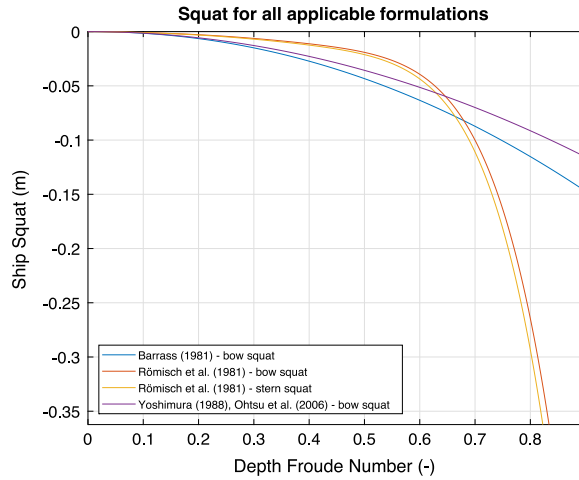


Fig. 15. In-house code output: Empirical formulae for channel 2.

Fig. 14 reveals that at $F_0 = 0.3$ the disturbance caused by the DTC is hardly noteworthy, furthermore, the waves generated can scarcely be attributed to have been created by a moving ship, however, a depression around the hull is observed. As we increase the velocity, several noticeable changes occur. Firstly, the well-known Kelvin wake is developed. The bow wave begins to interact with the waves shed from the stern. This is more prominent in Fig. 14 b and c. Furthermore, the transverse length of the waves increases as we move up the velocity scale. Secondly, a depression in the water is observed originating from the bow and ending rather sharply as the stern is approached. The phenomenon termed hull speed, observed by William Froude, states that a ship can appear to be trapped between two wave crests at the Hull speed/displacement velocity in knots, mathematically defined in Eq. (20).

$$V_h = 1.34\sqrt{L} \quad (20)$$

For the present case, after the units are converted into m/s, $V_h = 2.053$ m/s, which in terms of depth Froude number is $F_0 = 0.955$. Although the specific value has not been accounted for in the simulations carried out, the phenomenon has almost developed and is observable for $F_0 = 0.9$.

In Fig. 14a, b and c a depression is present in the areas adjacent to the walls on either side ahead of the bow. This is most likely attributable to the fact that the DTC modifies the velocity, elevation and pressure in a region extending forward of the bow. This is most prominent in the low speed range, however, its origin is most clear in the high end of F_0 .

An important observation from Fig. 14 is that the waves do not reflect from the side walls or interact with the ship hull in any way. Therefore, the dimension selection detailed in the previous section accomplished its objectives, namely, to approximate an infinitely wide shallow water region for this configuration.

Finally, the change in the wave patterns observed at $F_0 \geq 0.7$ coincides with the rapid change in the trend of the sinkage and trim values as shown in Fig. 12 and Fig. 13, respectively. As alluded to previously, a consensus exists when it comes to high speeds in shallow waters. Namely, the trim increases, while the sinkage decreases in relative importance. This statement is valid for the present case-studies.

5.1.2. Channel 2

In this section, the second case-study results are presented. For the two dredged channels (channel 2- $h_\infty/h_0 = 0.33$ and channel 3- $h_\infty/h_0 = 0.66$), only the empirical formulations which retain their validity for restricted configurations are applicable, as shown in Fig. 15. The first inference made here is regarding the results computed via the (Römisch et al., 1981) formulae for stern and bow squat. Due to the power at which the velocity is raised (34), the values become highly divergent towards the end of the velocity range.

The results computed via the Slender-Body theory for dredged channels and CFD are shown in Fig. 16.

The results for this case-study are of particular interest due to the exterior flow becoming supercritical ($F_\infty \rightarrow 1$) as $F_0 \rightarrow 0.6$. As before, the Slender-Body theory under predicts the CFD values throughout the majority of the range investigated due to the absence of non-linear and viscous terms in the theory. Similarly to the first case-study, the sinkage decreases in magnitude as the critical range is approached, as forecasted by Tuck (1966). In the present case-study, the sinkage curve slope is rapidly inverted after $F_0 = 0.6$. Comparing the trend exhibited by the sinkage values for channel 1 (Fig. 12) and the current case-study reveals the significant influence of the exterior dredged section.

The trim comparison between CFD and the Slender-body theory for channel 2 ($h_\infty/h_0 = 0.33$) is shown in Fig. 17.

In Fig. 17, the Slender-Body theory and CFD results seem to agree more in the low speed range when compared to channel 1, while the values computed for $F_0 = 0.6$ and $F_0 = 0.7$ do not follow this trend. This is most likely due to the

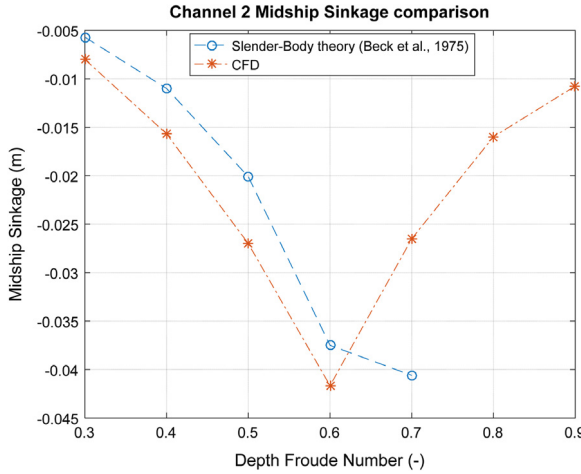


Fig. 16. CFD and Slender-Body theory comparison for channel 2.

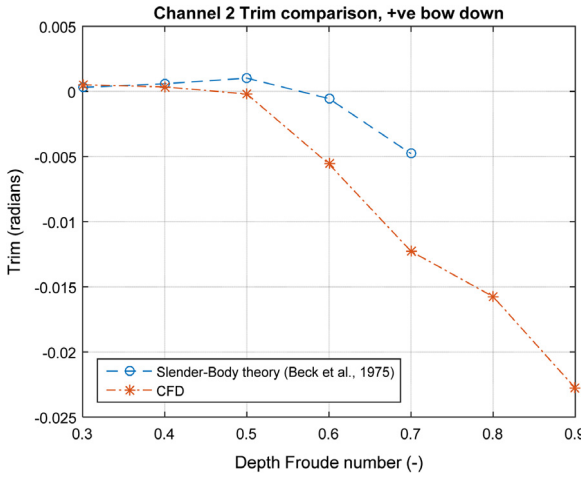


Fig. 17. Dynamic trim comparison for Channel 2; positive bow down.

exterior flow becoming supercritical at approximately $F_0 = 0.6$. The trim experienced by the DTC in the low speed range is significantly smaller, and changes from trim by bow to by stern much earlier than previously observed. Next, the wave elevation distributions in the computational domain are presented in Fig. 18.

In Fig. 18, dramatic changes are observed when compared to the channel 1 plot of wave elevation distributions (Fig. 14). Firstly, the step has a clear effect on the vertical displacement of the free surface. In Fig. 18 the water displacement is significantly influenced so that the position of the step is clearly visible around and ahead of the bow from the disturbance caused. Furthermore, the wave pattern behind the vessel is significantly modified by the depth discontinuity. As shown in Eq. (2), the wave velocity is expressed by $C = \sqrt{gh}$, where h is the water depth and g is the acceleration due to gravity. Now, in the interior region, this expression attains a higher value ($C_0 = \sqrt{gh_0}$) when compared to the exterior region ($C_\infty = \sqrt{gh_\infty}$). As a consequence of the change in wave velocity, the wake distribution is modified and does not closely resemble the expected Kelvin pattern. The change in speed is not the only outcome of the waves passing over the depth discontinuity. As alluded to in the section concerning the Slender-Body theoretical background, the waves refract from the step. The effect the transmitted component of the waves has on the overall wave field is most easily observable in Fig. 18b- where the contour lines change in intensity, the reflected wave has been superimposed on top of the existing wave in that region causing a larger amplitude where wave crests meet. Simultaneously, certain locations where some disturbance is expected, seem completely flat. In these areas, the reflected wave trough cancels out the wave crest resulting in the seemingly unaltered water surface. Finally, in Fig. 18c and d, the trim has caused the free surface to pierce the virtual towing tank bottom and is not shown in the scalar scenes above. This phenomenon is caused by the rotation of the domain with the DTC as explained in the previous sections. To show the original position of the free surface, the outline of the tank bottom has been made visible for both plots. The

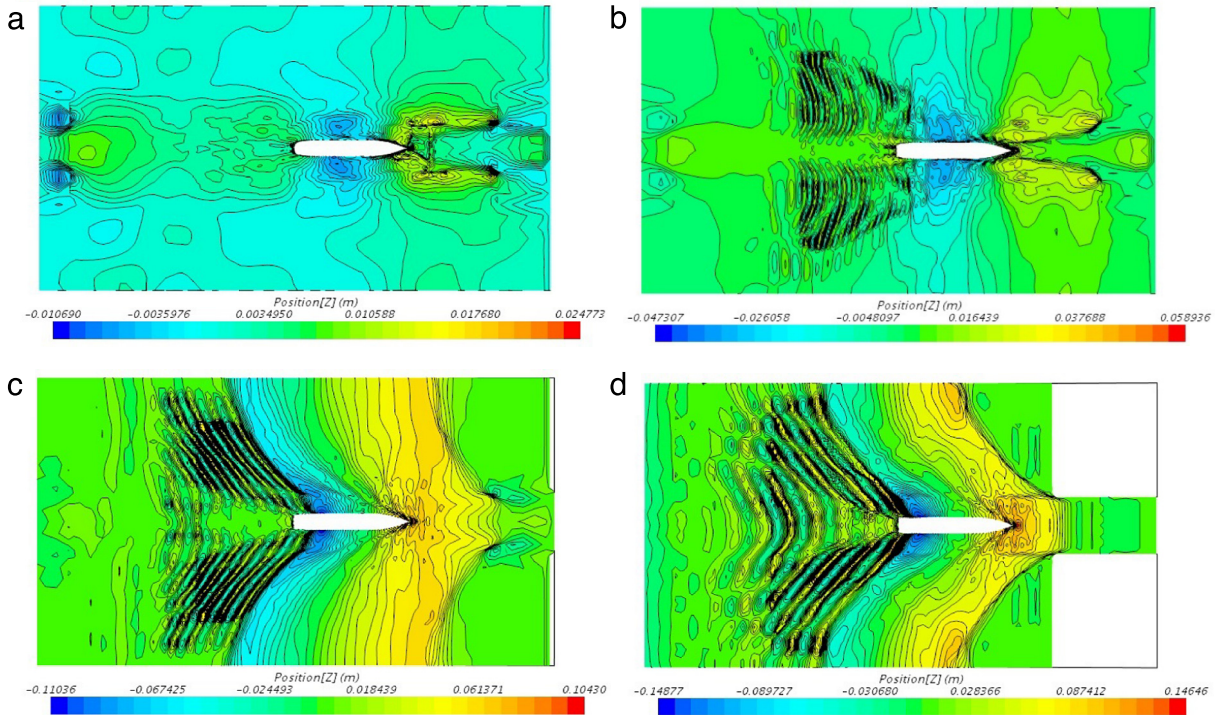


Fig. 18. Wave patterns; Channel 2 at $F_0 = \text{a}:0.3, \text{b}:0.5, \text{c}:0.7, \text{d}:0.9$.

pitch displacement seems to be more important in the higher end of the speeds investigated for channel 2 when compared to channel 1.

Finally, it is likely that the large displacement of the free surface under the computational domain has resulted in numerical inaccuracies. To elaborate, an insufficient section of the water surface has been modelled where the fluid interface is located beneath the computational domain. One way to tackle this would be imposing an overset mesh. In effect, this 'overlapping' or 'Chimera' mesh envelopes the moving body (in the current scenario, the DTC) into a finer resolution box-shaped mesh. The local coordinate system is then linked to this new region, rather than the entire computational domain, therefore, the influence of the large pitch displacement can be limited. However, in cases such as the one examined here, where the body is close to the boundaries of the domain, the overset mesh region is likely to collide with the towing tank bottom, thus rendering a similar result or causing the simulation to fail.

5.1.3. Channel 3

In this section, a case-study with a relatively deep exterior shallow water region ($h_\infty/h_0 = 0.66$) is presented. The applicable empirical formulae retaining their validity are the same as those shown in the previous section for channel 2, as shown in Fig. 19. As before, an upper limit equal to the ship's draught was set for the results computed via the (Römisch et al., 1981) formula. As shown in Figs. 19 and 15, the results are not highly affected by the change in the exterior shallow water region's depth according to the empirical formulae.

The midship sinkage comparison between the Slender-Body theory and CFD is shown in Fig. 20. The theory of Beck et al. (1975) behaves in a similar fashion as was the case for channel 2. The CFD results are underpredicted throughout the investigated velocity range, however, the difference seems to increase more in proportion as we progress towards the critical speed. This is likely since viscous and non-linear terms attain a higher relative importance than was the case for channel 2. The typical decrease in sinkage magnitude is observed as the velocity increases.

The trim comparison between CFD and the Slender-Body theory, for channel 3 is shown in Fig. 21.

A similar trend is observed as for the previous case study in Fig. 21. Namely, the trim distribution increases in magnitude as the velocity is increased. Furthermore, the two sets of data agree remarkably well in the low speed range. As the exterior flow becomes critical (at $F_0 \approx 0.8$), the trim begins to exhibit significant increase in amplitude. More specifically, it changes from by bow to by stern rather sharply and attains a large amplitude towards the high end of speeds investigated. In all likelihood, beyond $F_0 = 0.7$, nonlinear and hence viscous effects dominate the behaviour and performance of the DTC. Channel 3 also confirms the increase in relative importance of trim angles for high speeds in shallow waters. Finally, the wave elevation distributions are given in Fig. 22.

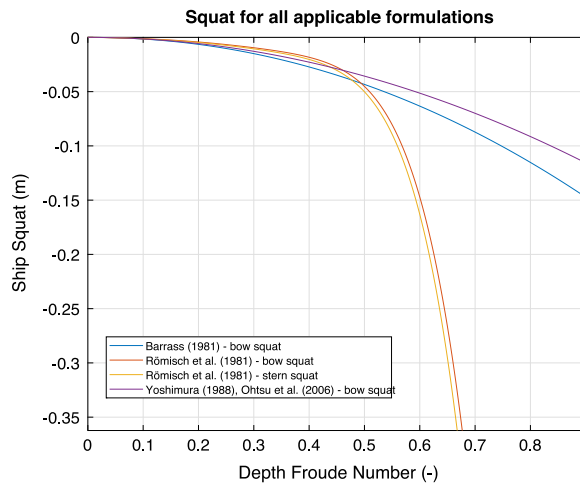


Fig. 19. In-house code output: Empirical formulae for channel 3.

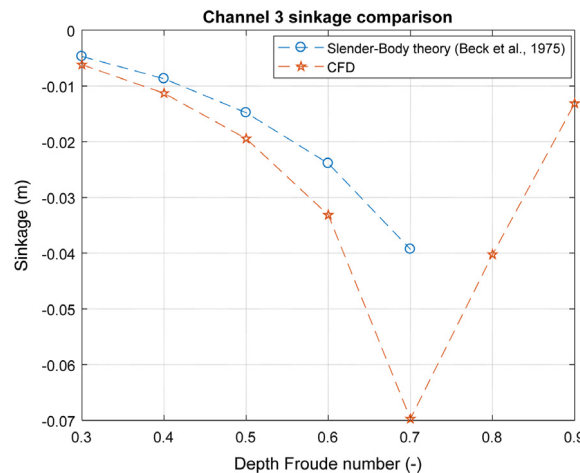


Fig. 20. CFD and Slender-Body theory comparison for channel 3.

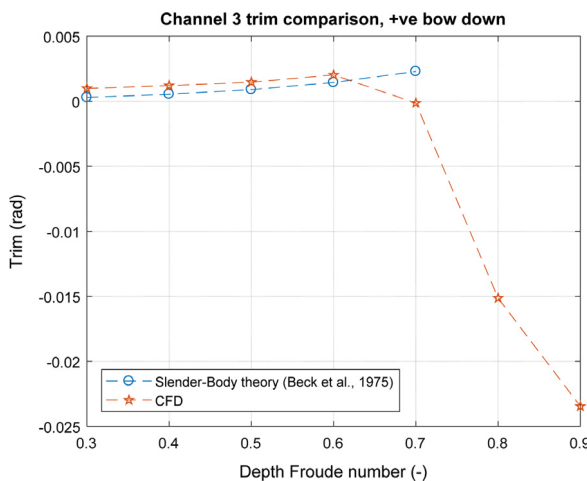


Fig. 21. Dynamic trim comparison for channel 3; positive bow down.

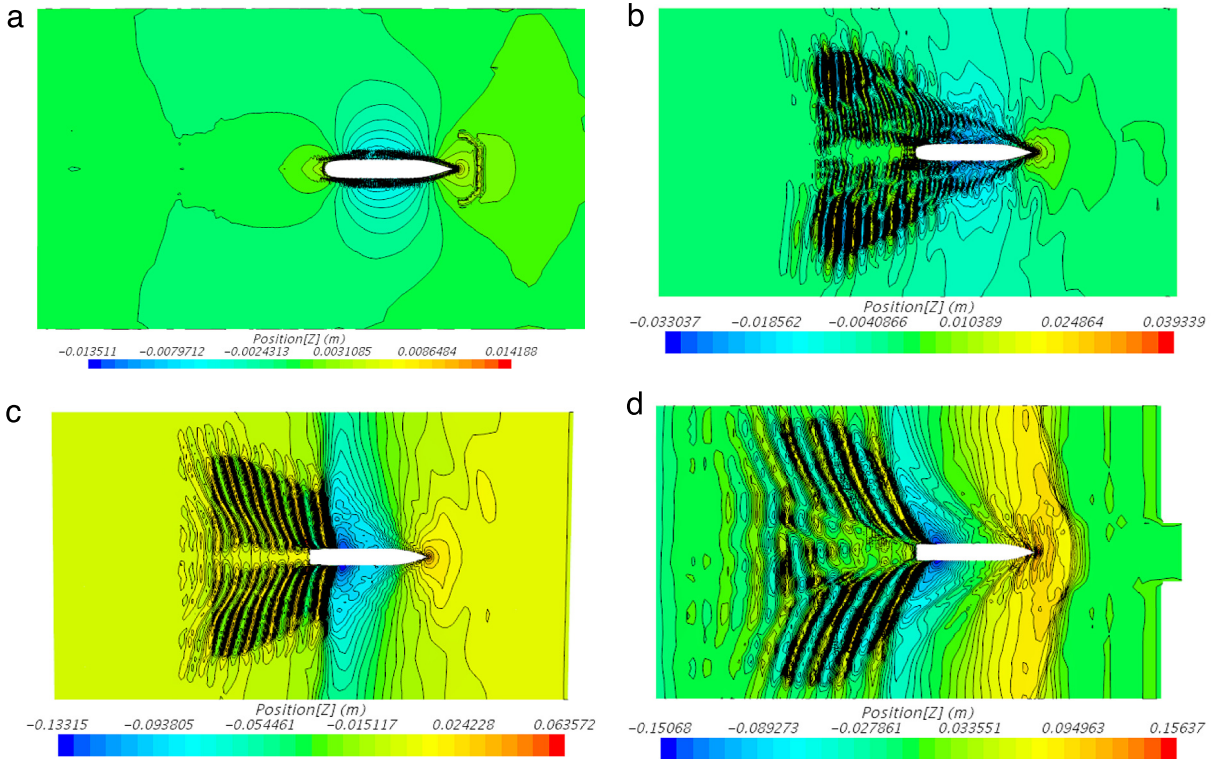


Fig. 22. Wave patterns; Channel 3 at $F_0 = \text{a}:0.3, \text{b}:0.5, \text{c}:0.7, \text{d}:0.9$.

Several interesting changes can be noted from the wave patterns of channel 3. In Fig. 22b the reinforcement and attenuation of waves caused by superimposing crest over crest or trough over crest, respectively, is different from Fig. 18b. More specifically, in Fig. 22b, the clustering of contour lines, i.e. the sharp gradients in the water surface elevation are more defined into groups, whereas in Fig. 18b, this distribution seems rather random. For $F_0 = 0.5$, the interaction of waves shed from the bow with those shed from the stern, and reflected from the step is evident. Secondly, the path the waves shed from the stern of the vessel in Fig. 22c and d follow a more linear path, without bending as much as in channel 2, as they progress over the exterior shallow water region. This is likely because of increased exterior water depth when compared to channel 2. Thirdly, the waves immediately behind the DTC are more pronounced and can be easily distinguished. Due to the trim, as was the case in Fig. 18, the free surface pierces the towing tank bottom and is not shown beyond this point.

5.1.4. Channel 4

For the final case-study, a scenario where a ship is advancing through a narrow canal is modelled. The empirical in-house code output for this configuration is shown in Fig. 23. Here, the divergent behaviour of the Römisich et al. (1981) formulae is more prominent in the low speed range, which is why the y-axis was limited as previously.

For this configuration, the theory developed by Tuck (1967) for restricted waters was employed by Slenderflow to produce the midship sinkage and trim, as shown in Fig. 24 and Fig. 25, respectively. As mentioned in the Background section, the Slender-Body theory is well suited for wide canals or open shallow waters at low speeds. However, the theory developed by Tuck (1967) seems to provide a good approximation to the CDF results throughout the majority of the range investigated, especially in the low speed range. As observed previously, the difference between the two sets of data increases as we progress through the velocity scale. Finally, the Slender-Body theory does not seem to predict the sharp decrease in sinkage at $F_0 = 0.7$. As the velocity is increased past this point, the vessel's CoG seems to rise out of the water, while the trim increases massively (Fig. 25).

The trim results predicted by the Slender-Body theory seem to be in best agreement with the CFD results for low speeds, when compared to the previous case-studies. However, the numerical output of Slenderflow does not predict the sharp changes in trim as we move past $F_0 = 0.6$. Finally, the wave patterns are shown in Fig. 26.

Once more, the outline of the virtual towing tank is shown in Fig. 26d, which has intersected the free surface much closer to the ship bow than in any previous case-study. In Fig. 26c the water surface is not sufficiently inclined relative to the bottom to pierce it, which is an unexpected result considering this has been the case for channels 2 and 3. For Fig. 26b it seems the reflection of the waves from the sides has caused the Hull speed to shift significantly to the lower velocity range and

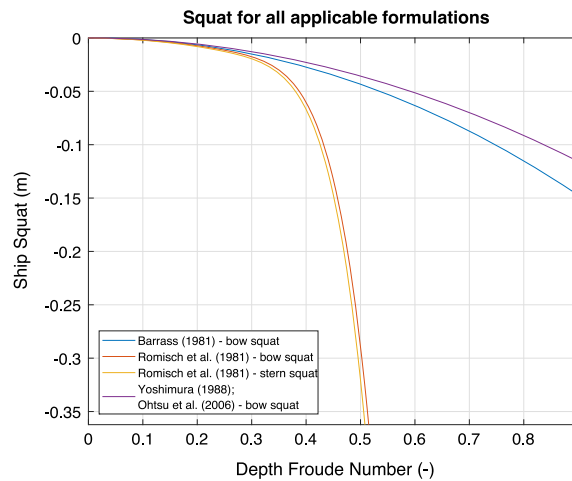


Fig. 23. In-house code output: Empirical formulae for channel 4.

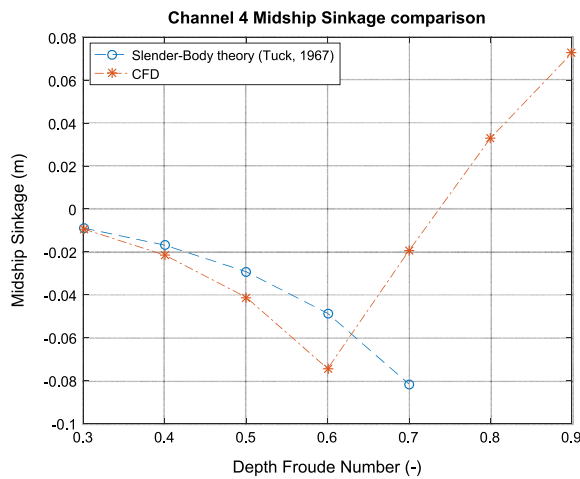


Fig. 24. CFD and Slender-Body theory comparison for channel 4.

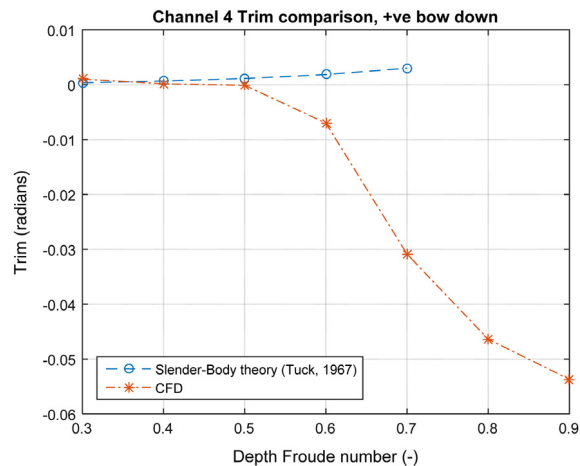


Fig. 25. Dynamic trim comparison for channel 4; positive bow down.

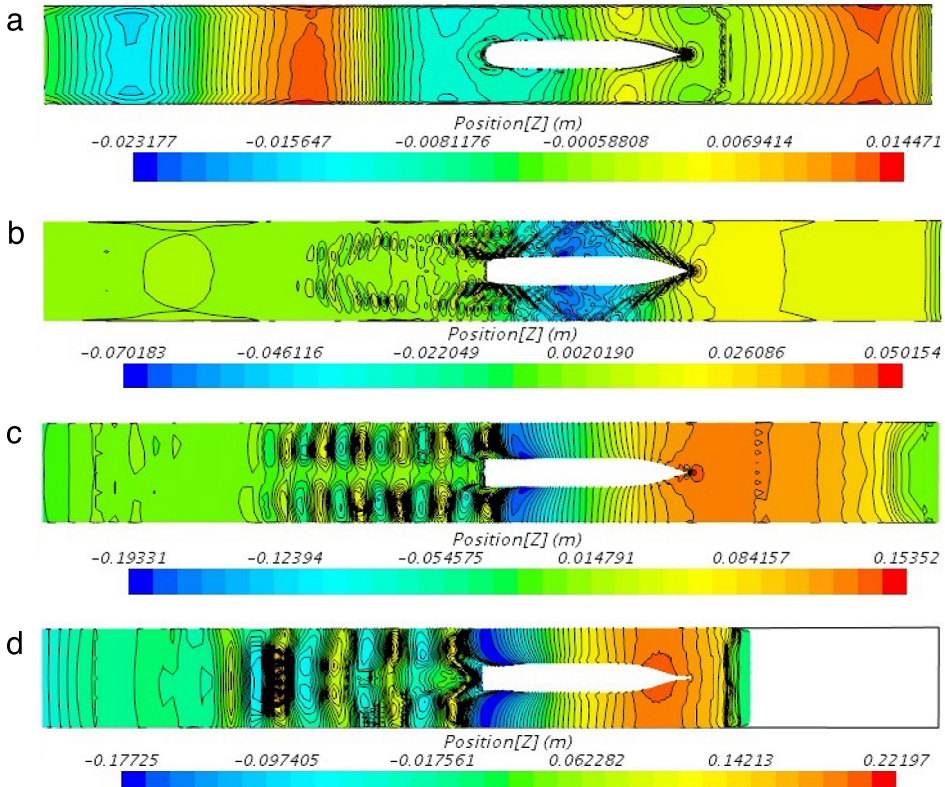


Fig. 26. Wave patterns; Channel 4 at $F_0 = \text{a}:0.3, \text{b}:0.5, \text{c}:0.7, \text{d}:0.9$.

for this depth Froude number and the DTC appears to be trapped between two wave crests. In contrast, when $F_0 = 0.9$, a concentrated depression which begins and ends sharply near the stern is observed, while the bow is located on the middle of a wave crest. For all speeds, except $F_0 = 0.5$, the DTC is followed by regular waves of different length. For the low speed range ($F_0 = 0.3$) the wavelength is larger than the vessel itself. This relationship changes rapidly as the speed is increased. In the plot for $F_0 = 0.5$, the trailing ripples are most likely caused by the waves generated by the DTC and their reflections.

5.2. Resistance coefficients

To assess the performance of a vessel, one of the key parameters designers and operators are interested in is the resistance characteristics. The resistance [N] of a ship can be broken down into several components. More specifically, frictional resistance (R_F) and pressure resistance (R_P), which can be further decomposed into wave making resistance (R_W) and viscous resistance (R_V). For the purposes of this paper, R_V and R_W are presented jointly as R_P . Then, the total resistance (R_T) is defined as shown in Eq. (21):

$$R_T = R_F + R_P \quad (21)$$

A more convenient way of presenting the resistance is in non-dimensional coefficient form. To achieve this, each component described above (Eq. (21)) is divided by $0.5\rho S_w V^2$, where S_w is the ship's wetted area. In this form, the performance of a ship can more easily be compared to other vessels. Once converted, the coefficients (C_F and C_P , respectively) are summed to give the total resistance coefficient (C_T) as shown in Eq. (22). This notation is used throughout this section for convenience and consistency.

$$C_T = C_F + C_P \quad (22)$$

To begin with, the resistance coefficients calculated using CFD are given for all configurations in Table 6. To put the shallow water region in perspective, in the table the F_∞ distribution of values is added where relevant.

Of particular interest are the values of the total resistance coefficient, because they show the overall performance of the ship, as looking at the broken-down components of resistance can sometimes be misleading. Beck et al. (1975) briefly discuss the effect of depth change of the exterior shallow water region and concludes that as h_∞ increases, resistance

Table 6Resistance coefficients ($\times 10^{-3}$) obtained using CFD.

	F_0	0.3	0.4	0.5	0.6	0.7	0.8	0.9
Channel 1	C_P	1.616	1.791	1.758	3.108	3.178	8.645	21.722
	C_F	3.519	3.456	3.354	3.439	3.447	3.846	3.589
	C_T	5.134	5.247	5.112	6.198	6.625	12.491	25.311
	F_∞	0.522	0.696	0.870	1.044	1.219	1.393	1.567
Channel 2	C_P	10.508	9.327	10.234	21.384	26.089	24.161	25.873
	C_F	5.123	4.727	4.793	4.541	3.689	3.222	3.330
	C_T	15.631	14.054	15.027	25.925	29.778	27.383	29.204
	F_∞	0.369	0.492	0.615	0.739	0.862	0.985	1.108
Channel 3	C_P	2.910	2.545	2.735	2.988	8.630	24.421	26.691
	C_F	3.527	3.453	3.373	3.455	4.025	3.618	3.383
	C_T	6.437	5.998	6.109	6.443	12.655	28.039	30.073
Channel 4	C_P	5.349	9.906	10.700	26.074	54.230	59.650	55.186
	C_F	4.331	4.505	4.611	5.563	5.751	5.120	4.558
	C_T	9.680	14.411	15.312	31.637	59.980	64.770	59.744

decreases. This statement is validated by the CFD results, but perhaps more importantly, this proves the assertion that the exterior region's depth has a significant impact on the resistance of a ship. Since the Slender-Body theory is linear, it is incapable of calculating the resistance, which is non-linear. Software such as Michlet can be used to estimate the resistance in shallow waters, however, it does not incorporate a dredged channel configuration, which is of greater interest. The total resistance coefficients are shown in Fig. 27, which presents highly interesting results. Namely, there is a dramatic difference in ship behaviour between case-studies. For instance, the total resistance coefficient of channel 1 describes a rather smooth quadratic curve. Channel 4 however, shows a sharp increase in magnitude at $F_0 = 0.7$. As the critical speed is approached, the resistance seems to decrease rather than increase. The two dredged case-studies also exhibit a different behaviour. For channel 2, the values decrease at $F_0 = 0.8$, only to increase as the critical value is approached. As reported in Castiglione et al. (2014), C_T shows higher peaks and increases in magnitude as the water depth decreases. For the case-studies incorporated here, it is shown that not only the depth, but width and channel cross-section are highly influential on the magnitude and peak of the resistance coefficient.

Table 6 shows the relative importance of the frictional resistance, which decreases rapidly as we move up the velocity scale. Contrarily, the pressure resistance begins dominating the total resistance after $F_0 = 0.6$. Table 6 highlights the change in resistance components as the channel topography changes.

Fig. 28 shows the sinkage distribution for all case-studies obtained using CFD. Several important conclusions can be drawn by comparing the sinkage curve of channels 2 and 4. As stated in Beck et al. (1975), modelling a canal case-study is equivalent to modelling one where the exterior water region has attained the critical value ($F_\infty = 1$), provided the width for both is the same. Examining the 'cusp' of each curve we note that for the two channels in question it is located at $F_0 = 0.6$. Now, according to Beck et al. (1975), both channels should have equivalent sinkage values at this depth Froude number. The discrepancy here is most likely due to the increasing importance of non-linear and viscous effects on the ship, especially around the critical speed.

For each channel, the cusp of the sinkage curve is a direct indication of where along the velocity scale the relative importance of sinkage and trim reverse. As the channel cross-section becomes more constrained, the cusp is located earlier. This suggests that reducing the channel cross-section, whether vertically or laterally, has a pronounced influence on the behaviour and performance of a ship.

5.3. Verification study

A crucial part of any study incorporating CFD methods is a proper verification study. In this section, the time step, and discretisation errors due to grid size induced by the numerical setup in Star-CCM+, are assessed based on case 10 (Channel 2, $F_0 = 0.5$).

As stated by Xing and Stern (2010), the Richardson extrapolation (RE) method (Richardson, 1911) is the current basis for quantifying numerical uncertainty. The error is expanded in a power series with integers of powers of grid spacing or time step as a finite sum. Assuming the solutions lie in the asymptotic range, only the first term is taken, which leads to the so-called grid triplet study. Furthermore, according to Xing and Stern (2010), the grid convergence index (GCI), derived by Roache (1998) can be used to estimate uncertainties due to grid spacing and time-step errors and is widely used.

As in Tezdogan et al. (2016), the procedure of Roy and Blottner (2001) was used to predict iterative errors. The calculations suggest that the iterative errors are equal to almost zero for squat and resistance values.

Firstly, to assess the convergence condition, the convergence ratio (R_k) is defined as the difference (ε_{k21}) between the medium and fine ($\varphi_{k2} - \varphi_{k1}$) solutions, and the difference between the (ε_{k32}) coarse and medium solutions ($\varphi_{k3} - \varphi_{k2}$). Here, the subscript k is used to describe the k th input parameter (Stern et al., 2006).

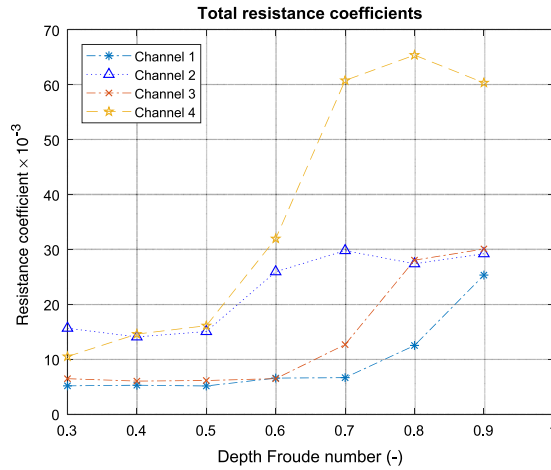


Fig. 27. Total resistance coefficients ($\times 10^3$) for the four different channel configurations obtained using CFD.

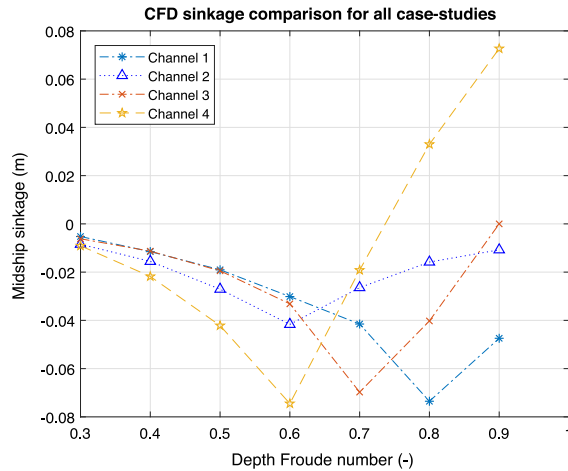


Fig. 28. CFD sinkage comparison for all case studies.

The typical convergence conditions are defined as (Stern et al., 2006):

1. Monotonic convergence, where $0 < R_k < 1$
2. Oscillatory convergence, where $R_k < 0$ and $|R_k| < 1$
3. Monotonic divergence, where $R_k > 1$
4. Neither error nor uncertainty can be evaluated

The generalised RE method is used to evaluate the order of accuracy (p_k) of the k th input as defined in Celik et al. (2008).

$$p_k = \frac{\ln(\varepsilon_{k23}/\varepsilon_{k21})}{\ln(r_k)} \quad (23)$$

The next step is to calculate the extrapolated values:

$$\Phi_{ext}^{21} = (r_k^p - \Phi_1 - \Phi_2)/(r_k^p - 1) \quad (24)$$

Then, the approximate relative error and extrapolated relative error are Eq. (25) and Eq. (26), respectively:

$$e_a^{21} = \left| \frac{\Phi_1 - \Phi_2}{\Phi_1} \right| \quad (25)$$

$$e_{ext}^{21} = \left| \frac{\Phi_{ext}^{21} - \Phi_1}{\Phi_{ext}^{12}} \right| \quad (26)$$

Table 7

Grid convergence study for sinkage and total resistance coefficient.

	Sinkage at CoG (with monotonic convergence)	C_T (with monotonic convergence)
r	$\sqrt{2}$	$\sqrt{2}$
φ_1	-0.027	14.844×10^{-3}
φ_2	-0.028	13.724×10^{-3}
φ_3	-0.033	10.148×10^{-3}
R	0.2	0.3132
p	4.6439	3.3497
φ_{ext}^{21}	-0.02675	0.015355
$e_a^{21} (\%)$	3.70	7.55
$e_{ext}^{21} (\%)$	0.93	3.32
$GCI_{fine}^{21} (\%)$	1.16	4.30

Table 8

Time step convergence study for sinkage and total resistance coefficient.

	Sinkage at CoG (with monotonic convergence)	C_T (with monotonic convergence)
r	$\sqrt{2}$	$\sqrt{2}$
φ_1	-0.027	14.844×10^{-3}
φ_2	-0.026	14.831×10^{-3}
φ_3	-0.023	14.804×10^{-3}
R	0.333	0.4815
p	3.1699	2.1089
φ_{ext}^{21}	-0.0275	0.014856
$e_a^{21} (\%)$	3.70	0.09
$e_{ext}^{21} (\%)$	1.82	0.08
$GCI_{fine}^{21} (\%)$	2.31	0.10

The process described in this section is only valid for a constant r_k value. All notations have been adopted from Celik et al. (2008) to alleviate verification and presentation of the results.

The equations above lead to the fine-grid convergence index, defined by:

$$GCI_{fine}^{21} = \frac{1.25e_a^{21}}{r_k^p - 1} \quad (27)$$

The grid convergence study was conducted using three calculations in which the grid size was systematically coarsened in all directions whilst keeping all other input parameters (such as time-step) constant. The mesh convergence analysis was carried out with the smallest time-step, whereas the time-step convergence analysis was carried out with the finest grid size. The same procedure was also applied in Kavli et al. (2017) and Demirel et al. (2017). It should be noted that the finest mesh resolution with details given in Table 5 was applied throughout all cases investigated in this work. As a starting point in the mesh convergence and time step studies, a refinement ratio equal to $\sqrt{2}$ was selected. To maintain the accurate representation of the ship hull throughout the mesh convergence studies, the surface mesh properties were kept constant. The results from the mesh convergence study are shown in Tables 7 and 8.

6. Concluding remarks and future work

As part of this study, empirical, analytical and unsteady RANS methods were employed to predict the sinkage, trim and resistance of the DTC advancing through a variety of channels at a wide range of speeds. An attempt was made to approximate an infinitely wide shallow water case-study in Star-CCM+, which was shown to be successful by the generated wave patterns. Two dredged channels of varying exterior depth were modelled in order to quantify the effect of the step on ship behaviour and performance. A canal case-study was also adopted to show the restricted width effects on the parameters of interest.

The results show good agreement between empirical formulae, Slender-Body theory and CFD in the low speed range. As we move up the velocity scale, some disagreement is present between the Slender-Body theory and CFD results, attributable to the neglect of viscous and non-linear terms by the Slender-Body theory.

The assertion that sinkage is important in the low speed range, whereas trim is the leading factor in the high-speed range was shown to hold for all case-studies. Resistance was also revealed to be highly sensitive to changes in the underwater topography of the channel.

The hypothesis of Beck et al. (1975), according to whom the resistance of a ship decreases as the exterior depth (h_∞) increases in a dredged channel, was proven via our CFD results. Furthermore, the components of the total resistance were shown to vary dramatically between case-studies.

This research has revealed the importance of width and channel dredging on ship sinkage, trim and resistance. Channel 1 was shown to provide the most moderate results across the parameters investigated, especially when compared to channel 4. The final case-study, proved to influence the trim and resistance to a much higher degree than any other channel.

One of the key finding of the Pre-Squat workshop was the effect of turbulence modelling on ship resistance in shallow water areas. As discussed in Yahfoufi and Deng (2014)'s study presented at the workshop, turbulence modelling influences resistance predictions in shallow waters by 3%–5%. At low UKC, the relative importance of turbulence modelling is higher at low speeds. The sensitivity of the solution to turbulence modelling can be explained by the fact of flow separation at the stern. As acknowledged by Yahfoufi and Deng (2014), a systematic study with comparison to experimental data is required to accurately predict the effect of turbulence modelling on ship squat and resistance. As there are no experimental studies currently, this has been suggested as a future study for researchers studying in this area.

The shallow water behaviour and performance of large ships will undoubtedly become more important as the world fleet undergoes modernisation. Projects such as the one commissioned by Norway require more in-depth knowledge and research in this field.

This paper has provided a strong basis from which further investigations into the behaviour and performance of ships in shallow water can benefit. The research conducted here could be extended by altering the draught of the ship or the relative position of the ship's centreline to that of the channel/canal as in Beck (1977).

Self-propulsion is also known to have the effect of re-energising the boundary layer near the stern, which may affect the results (Gourlay et al., 2015). In any case, experimental studies incorporating dredged channels would be most beneficial for future developments in the field.

Acknowledgements

The authors are grateful for the EPSRC's support for the project on 'Shipping in Changing Climates' (EPSRC Grant No. EP/K039253/1) which enabled them to carry out the research reported in this paper.

It should be noted that the results were obtained using the EPSRC funded ARCHIE-WeSt High Performance Computer (www.archiewest.ac.uk). EPSRC grant no. EP/K000586/1. The underlying data in this paper is openly available from the University of Strathclyde data repository at: <http://dx.doi.org/10.15129/b094fbee-cfd4-4ed8-b2cc-551108c67d70>.

Appendix

Parameter	Symbol	Unit	Formula	Notes
Bow Squat (Barrass, 1981)	S_b	m	$\frac{C_b S_2^{2/3} V^{2.08}}{30}$	
Velocity return factor	S_2	—	$\frac{A_s}{A_c - A_s}$	
Blockage factor	S	—	$\frac{A_s}{A_c}$	
Channel cross-sectional area	A_c	m^2		
Ship cross sectional area	A_s	m^2		
Bow squat (Eryuzlu and Hausser, 1978)	S_b	m	$0.113B\left(\frac{1}{h/T}\right)^{0.27} F_d^{1.8}$	
Bow squat (Eryuzlu et al., 1994)	S_b	m	$0.298 \frac{h^2}{T} \left(\frac{V}{\sqrt{gT}}\right)^{2.289} \left(\frac{h}{T}\right)^{-2.972} K_b$	
Correction factor	K_b	—	$\frac{3.1}{\sqrt{W/B}}$ for $W/B < 9.61 = 1$ for $W/B \geq 9.61$	For unrestricted channels, use W_{eff} – effective width (31)
Effective width	W_{eff}	m	$C_M B = [7.7 + 45(1 - C_{WP})^2] (31)$	
Bow squat (Hooft, 1974)	S_b	m	$1.96 \frac{\nabla}{l^2} \frac{F_d^2}{\sqrt{1-F_d^2}}$	∇ is the volumetric displacement
Bow squat (ICORELS, 1980)	S_b	m	$2.4 \frac{\nabla}{l^2} \frac{F_d^2}{\sqrt{1-F_d^2}}$	
Bow squat (Millward, 1990, 1992)	S_b	m	$0.001L(61.7C_b \frac{1}{L/B} - 0.6) \frac{F_d^2}{\sqrt{1-0.9F_d^2}}$	
Bow squat (Römisch et al., 1981)	S_b	m	$C_V C_F K_T T (32)$	
Stern squat (Römisch et al., 1981)	S_s	m	$C_V K_T T (33)$	

(continued)

Parameter	Symbol	Unit	Formula	Notes
Correction factor	C_V	—	$8\left(\frac{V}{V_{CR}}\right)^2 \left[\left(\left(\frac{V}{V_{CR}} - 0.5 \right)^4 + 0.0625 \right) \right]$ (34)	For ship speed
Relevant water depth	h_{mT}	m	$h - \frac{h_m}{h}(h - h_m)$	
Wave celerity	C_{mT}	$\frac{m}{s}$	$\sqrt{gh_{mT}}$	Based on the relevant water depth
Mean water depth	h_m	m	$\frac{A_c}{W_{Top}}$	
Channel width	W_{Top}	m	$W + 2nh$	At the water surface
Correction factor for the ship's shape	C_F	—	$\left(\frac{10C_b}{L/B}\right)^2$	= 1 for stern squat
Correction factor	K_T	—	$0.155\sqrt{h/T}$	For squat at critical speeds
Wave celerity	C	$\frac{m}{s}$	\sqrt{gh}	Based on the depth h
Inverse bank slope	n	—	—	Specified as an integer
Ship critical speed	V_{CR}	$\frac{m}{s}$	$V_{CR} = CK_{ch}$ $V_{CR} = CK_C$	U configurations R configurations C configurations
Correction factor	K_c	—	$V_{CR} = \frac{C_{mT} \left[K_{ch} \left(1 - \frac{h_m}{h} + K_c \left(\frac{h_m}{h} \right) \right) \right]}{0.2306 \log \left(\frac{1}{S} \right) + 0.0447}$	
Wave celerity	C_{mT}	$\frac{m}{s}$	$\sqrt{gh_{mT}}$	Based on the relevant water depth h_{mT}
Bow/Stern squat (Ankudinov et al., 1996)	S_{Max}	m	$L(S_{mid} \pm 0.5Trim)$ +0.5Trim: Bow -0.5Trim: Stern	Bow/Stern squat depends on trim (+/-). For $F_d \leq 0.6$
Midship sinkage (Ankudinov et al., 1996)	S_{mid}	m	$(1 + K_p^S)P_{Hu}P_{Fd}P_{+h/T}P_{Ch1}$	For $F_d \leq 0.6$
Factor	K_p^S	—	0.15 0.13	Ships with single propellers Ships with twin propellers
Hull parameter	P_{Hu}	—	$1.7C_B \left(\frac{B/T}{L^2} \right) + 0.004C_b^2$	
Forward speed parameter	P_{Fd}	—	$F_d^{1.8+0.4F_d}$	
Water depths effect parameter	$P_{+h/T}$	—	$01 + \frac{0.35}{(h/T)^2}$	
Channel effects parameter	P_{Ch1}	—	1 $1 + 10S_h - 1.5(1 + S_h)\sqrt{S_h}$	U configurations R and C configurations
Water depth factor	S_h	—	$C_B \left(\frac{S}{h/T} \right) \left(\frac{h_T}{T} \right)$ $- 1.7P_{Hu}P_{Fd}P_{h/T}K_{Tr}P_{Ch2}$	R and C configurations
Trim (Ankudinov et al., 1996)	Trim	°		
Trim coefficient	K_{Tr}	—	$C_b^{nTr} - (0.15K_p^S + K_p^T) -$ $(K_B^T + K_{Tr}^T + K_{T1}^T)$ $2 + 0.8P_{Ch1}/C_b$	
Trim exponent	n_{TR}	—		
Propeller parameter	K_p^T	—	0.15 0.2	Single propellers Twin propellers
Bulbous bow parameter	K_B^T	—	0.1 0	Ships with bulbous bows Ships without bulbous bows
Stern transom parameter	K_{Tr}^T	—	0.04 0	Ships with a stern transom Ships without a stern transom
Initial trim factor	K_{T1}^T	—	$\frac{T_{ap} - T_{fp}}{T_{ap} + T_{fp}}$	
Trim correction parameter	P_{Ch2}	—	1 $1 - 5S_h$	U configurations R and C configurations

(continued)

Parameter	Symbol	Unit	Formula	Notes
Bow squat (Yoshimura, 1988)	S_b	m	$\left[\left(0.7 + \frac{1.5T}{h} \right) \left(\frac{BC_b}{L} \right) + \frac{15T}{h} \left(\frac{BC_b}{L} \right)^3 \right] V_e^2$	U, R and C configurations $g = 9.81 \text{ m/s}$
Enhanced ship speed term	V_e	$\frac{\text{m}}{\text{s}}$	$\frac{V}{1-S}$	

References

- Alderf, N., Lefrançois, E., Sergent, P., Debaillon, P., 2011. Dynamic ship response integration for numerical prediction of squat in highly restricted waterways. *Internat. J. Numer. Methods Fluids* 65, 743–763.
- Alidadi, M., Caisal, S., 2011. A numerical study on squat of a wigley hull. In: ASME 30th International Conference on Ocean, Offshore and Arctic Engineering. American Society of Mechanical Engineers, pp. 539–543.
- Ankudinov, V., Daggett, L., Huval, C., Hewlett, C., 1996. Squat predictions for maneuvering applications. In: International Conference on Marine Simulation and Ship Maneuverability, MARSIM'96, pp. 467–495.
- Barrass, C., 1981. Squat- a reply to a comparison of 2 prediction methods. *Nav. Archit.* E268–E271.
- Barrass, C., 2012. Ship Squat in Open Water and in Confined Channels-Chapter 17.
- Beck, R.F., 1977. Forces and moments on a ship moving in a shallow channel. *J. Ship Res.* 21 (2), 107–119.
- Beck, R.F., Newman, J.N., Tuck, E.O., 1975. Hydrodynamic forces on ships in dredged channels. *J. Ship Res.* 19 (3), 166–171.
- Briggs, M.J., 2009. Ankudinov Ship Squat Predictions-Part 1: Theory, Parameters, and FORTRAN Programs. DTIC Document.
- Briggs, M.J., 2006. Ship squat predictions for ship/tow simulator. DTIC Document.
- Castiglione, T., He, W., Stern, F., Bova, S., 2014. URANS simulations of catamaran interference in shallow water. *J. Mar. Sci. Technol.* 19 (1), 33–51. <http://dx.doi.org/10.1007/s00773-013-0230-5>.
- CD-ADAPCO, 2016. Star-CCM+ User Guide 11.02. USA.
- Celik, I.B., Ghia, U., Roache, P.J., 2008. Procedure for estimation and reporting of uncertainty due to discretization in CFD applications. *Trans. ASME, J. Fluids Eng.* 130.
- Constantine, T., 1960. On the movement of ships in restricted waterways. *J. Fluid Mech.* 9, 247–256.
- Debaillon, P., 2010. Numerical investigation to predict ship squat. *J. Ship Res.* 54, 133–140.
- Demirbilek, Z., Sargent, F., 1999. Deep-Drift Coastal Navigation Entrance Channel Practice. Coastal Engineering Technical Note CETN I-63. US Army Engineer Research and Development Center, Vicksburg, MS. <http://bigfoot.wes.army.mil/cetn/index.html>.
- Demirel, Y.K., Turan, O., Inceciik, A., 2017. Predicting the effect of biofouling on ship resistance using CFD. *Appl. Ocean Res.* 62, 100–118. <http://dx.doi.org/10.1016/j.apor.2016.12.003>.
- El-Mohtar, O.E., Shigunov, V., Zorn, T., 2012. Duisburg test case: Post-panamax container ship for benchmarking. *Ship Technol. Res.* 59, 50–64.
- Eryuzlu, N., Cao, Y., D'Agnolo, F., 1994. Underkeel requirements for large vessels in shallow waterways. In: PIANC Proceedings 28th International Congress, Section II, Subject.
- Eryuzlu, N., Haussner, R., 1978. Experimental investigation into some aspects of large vessel navigation in restricted waterways. In: Symp Proc on Asp of Nav of Constraint Waterways.
- Feng, A., Bai, W., You, Y., Chen, Z.-M., Price, W., 2016. A rankine source method solution of a finite depth, wave–body interaction problem. *J. Fluids Struct.* 62, 14–32.
- Gourlay, T., 2007. Ship underkeel clearance in waves. In: Proc. Coasts and Ports, Melbourne, p. 15.
- Gourlay, T., 2008. Slender-body methods for predicting ship squat. *Ocean Eng.* 35, 191–200.
- Gourlay, T., 2009. Sankage and trim of two ships passing each other on parallel courses. *Ocean Eng.* 36, 1119–1127.
- Gourlay, T.P., Ha, J.H., Mucha, P., Uliczka, K., 2015. Sankage and trim of modern container ships in shallow water. In: 22nd Australasian Coastal and Ocean Engineering Conference and the 15th Australasian Port and Harbour Conference, 2015. Engineers Australia and IPENZ, p. 344.
- Ha, J.H., Gourlay, T.P., 2017. Validation of container ship squat modelling using full-scale trials at the port of fremantle. *J. Waterway Port Coast. Ocean Eng.* (in press).
- Havelock, T.H., 1908. The propagation of groups of waves in dispersive media, with application to waves on water produced by a travelling disturbance. *Proc. R. Soc. Lond. Ser. A* 81, 398–430.
- Holtrop, J., 1978. A statistical power prediction method. *Int. Shipbuild. Prog.* 25.
- Hooth, J., 1974. The Behaviour of a Ship in Head Waves At Restricted Water Depths. NASA STI/Recon Technical Report N, 75.
- ICORELS, 1980. Report of Working Group IV. PIANC, Bulletin No. 35.
- Inui, T., 1954. Wave-making resistance in shallow sea and in restricted water, with special reference to its discontinuities. *J. Zosen Koikai* 1954, 1–10.
- ITTC, 2011. Practical Guidelines for Ship CFD Applications. ITTC.
- Jachowski, J., 2008. Assessment of ship squat in shallow water using CFD. *Arch. Civ. Mech. Eng.* 8, 27–36.
- Janssen, P., Schijf, J., 1953. The relation between the form of cross section the cross section, the method of revetment and the distribution of the water velocities in a waterway. In: PIANC.
- Joukovski, N., 1903. On the wave of translation. Complete Works 4.
- Kavli, H.P., Tezdogan, T., Oguz, E., 2017. A comparative study on the design of an environmentally friendly RoPax ferry using CFD. *Ocean Eng.* 137, 22–37. <http://dx.doi.org/10.1016/j.oceaneng.2017.03.043>.
- Kreitner, J., 1934. The Resistance of Ships in Confined Waters. Werft-Rederei-Hafen.
- Lewis, E.V., 1988. Principles of Naval Architecture Second Revision. SNAME, Jersey.
- Michell, J.H., 1898. XI. the wave-resistance of a ship. *Lond. Edinb. Dublin Philos. Mag. J. Sci.* 45, 106–123.
- Millward, A., 1990. A preliminary design method for the prediction of squat in shallow water. *Mar. Technol.* 27, 10–19.
- Millward, A., 1992. A comparison of the theoretical and empirical prediction of squat in shallow water.
- Mucha, P., El-Mohtar, O.E., 2014. Numerical prediction of resistance and squat for a containership on shallow water. In: 17th Numerical Towing Tank Symposium, Marstrand, Sweden, September 2014.
- Mucha, P., El-Mohtar, O.E., Bottner, C.U., 2014. Technical note: PreSquat - Workshop on numerical prediction of ship squat in restricted waters. *Ship Technol. Res. Schiffstechnik* 61 (3), 162–165.
- Norrbom, N.H., 1986. Fairway design with respect to ship dynamics and operational requirements (No. SSPA-RR-102).
- Ohtsu, K., Yoshimura, Y., Hirano, M., Tsugane, M., Takahashi, H., 2006. Design standard for fairway in next generation. In: Asia Navigation Conference.
- Perry, J., 2017. Norway to spend \$315M on world's first ship tunnel. CNN.

- PIANC, 1997. Approach Channels A Guide for Design. Final Report, PIANC Bulletin 95.
- Prabhakara, S., Deshpande, M., 2004. The no-slip boundary condition in fluid mechanics. *Resonance* 9, 61–71.
- Prakash, S., Chandra, B., 2013. Numerical estimation of shallow water resistance of a river-sea ship using CFD. *Int. J. Comput. Appl.* 71.
- Quérard, A., Temarel, P., Turnock, S., 2008. Influence of viscous effects on the hydrodynamics of ship-like sections undergoing symmetric and anti-symmetric motions, using RANS. In: ASME 2008 27th International Conference on Offshore Mechanics and Arctic Engineering, 2008. American Society of Mechanical Engineers, pp. 683–692.
- Richardson, L.F., 1911. The approximate arithmetical solution by finite differences of physical problems involving differential equations, with an application to the stresses in a masonry dam. *Phil. Trans. R. Soc. A* 210, 307–357.
- Roache, P.J., 1998. Verification and validation in computational science and engineering, Hermosa Albuquerque, NM.
- Roy, C.J., Blottner, F.G., 2001. Assessment of one-and two-equation turbulence models for hypersonic transitional flows. *J. Spacecr. Rockets* 38, 699–710.
- Römisch, K., Fuehrer, M., Engelke, G., 1981. Criteria for dimensioning the bottom and slope protection and for applying the new methods of protecting navigation canals. In: 25th International Navigation Congress, Permanent International Association of Navigation Congresses.
- Stern, F., Wilson, R., Shao, J., 2006. Quantitative V&V of CFD simulations and certification of CFD codes. *Internat. J. Numer. Methods Fluids* 50, 1335–1355.
- Tezdogan, T., 2015. Potential and CFD-based hydrodynamic analyses of mono- and multi-hull vessels (Ph.D.thesis), University of Strathclyde, Glasgow.
- Tezdogan, T., Demirel, Y.K., Kellett, P., Khorasanchi, M., Incecik, A., Turan, O., 2015. Full-scale unsteady RANS CFD simulations of ship behaviour and performance in head seas due to slow steaming. *Ocean Eng.* 97, 186–206.
- Tezdogan, T., Incecik, A., Turan, O., 2016. A numerical investigation of the squat and resistance of ships advancing through a canal using CFD. *J. Mar. Sci. Technol.* 21, 86–101.
- Tuck, E., 1966. Shallow-water flows past slender bodies. *J. Fluid Mech.* 26, 81–95.
- Tuck, E., 1967. Sinkage and trim in shallow water of finite width. *Schiffstechnik* 14.
- Uliczka, K., (2010) Fahrdynamisches Verhalten eines groben Containerschiffs in seiten- und tiefenbegrenztem Fahrwasser. Bundesanstalt für Wasserbau, Hamburg.
- Wang, H., Rutherford, D., Desai, C., 2014. Long-Term Energy Efficiency Improvement for LNG carriers. International Council on Clean Transportation.
- Wortley, S., 2013. CFD Analysis of Container Ship Sinkage, Trim and Resistance. B. Eng Mechanical Engineering Project Report.
- Xing, T., Stern, F., 2010. Factors of safety for Richardson extrapolation. *J. Fluids Eng.* 132, 061403.
- Yahfoufi, N., Deng, G., 2014. Resistance prediction of the DTC container ship model in shallow water. In: Mucha, P., El-Mohtar, O. (Eds.), Proceedings, PreSquat – Numerische Vorhersagen Von Dynamischem Squat in Begrenzten Gewässern, Bericht F005/2014. Institut für Schiffstechnik, Universität Duisburg-Essen.
- Yao, J.-X., Zou, Z.-J., 2010. Calculation of ship squat in restricted waterways by using a 3D panel method. *J. Hydrodynam. B* 22, 489–494.
- Yasukawa, H., 1993. A Rankine panel method to calculate steady wave-making resistance of a ship taking the effect of sinkage and trim into account.
- Yoshimura, Y., 1988. Mathematical model for the manoeuvring ship motion in shallow water, 2nd report: Mathematical model at slow forward speed. *J. Kansai Soc. Nav. Archit.*